Unit of Applied Mechanics
University of Innsbruck

Final Report for the Marshall Plan Scholarship

Vertical Acceleration Demands on Nonstructural Components in Buildings

Lukas Moschen

July 4, 2014

Advisors

Ricardo A. Medina
Department of Civil Engineering
University of New Hampshire

Christoph Adam
Unit of Applied Mechanics
University of Innsbruck

Acknowledgement

This report is the result of the scientific activities during my stay in the Department of Civil Engineering at the University of New Hampshire in Durham. The financial support of the Marshall Plan Foundation is gratefully acknowledged.

I would like to thank my advisors Professor Christoph Adam and Professor Ricardo A. Medina who gave me the possibility to expand my academic, professional, as wells as personal horizon.

Special thanks go to Shokoufeh Zargar, Miguel Negrete-Padilla, and Rui Zhang who made my stay in the U.S. an unforgettable time in my life. Thank you for your friendship these days!

The support of Sandra E. Scherl who guided me through the application process of the Marshall Plan Scholarship and the U.S. visa procedure is gratefully acknowledged.

Last but not least I would, like to thank my parents for their help from every point of view as well as my friends for their patience during this time period.

Contents

List of Figures

List of Tables

1 Introduction

Many studies have been conducted during the last decades to assess seismic acceleration demands on nonstructural components (NSCs, also named secondary structures, building contents, mechanical an electrical equipment, architectural components) attached to elastic and inelastic buildings. Most research activities have focused on the horizontal acceleration components of ground motion. As a result, design engineers have relied upon simplified equations provided by building codes [1–3] to estimate the maximum horizontal acceleration demands on NSCs with much less attention been paid to maximum vertical acceleration demands.

Currently, a relatively small number of studies incorporates the effect of the vertical component of ground motion and its corresponding vertical floor motions. Generally, structural systems commonly used in buildings are considered to be relatively flexible in the lateral direction and relatively rigid in the vertical (longitudinal) direction. If columns were axially rigid, negligible amplification of the vertical component of the ground motion would occur for NSCs located at or near columns. On the other hand, for NSCs located at open-bays, i.e., at locations away from columns and relatively close to girders or in the middle of slabs, an amplification of the vertical floor acceleration with respect to ground has the potential to be significant. This is due to resonance effects due to the out-of-plane flexibility of the girder/slab and the frequency content of the base excitation [4]. Therefore, vertical floor accelerations are highly dependent on the location of the component in a specific floor, the location of the component along the height of the building, and the characteristics and properties of the floor system.

For NSCs of various frequencies a rigorous and comprehensive evaluation of their response must consider floor response spectra. This is particularly important given the myriad of periods (in this case horizontal vibration periods) associated with secondary structures such as electrical and mechanical equipment. These systems are generally classified as acceleration-sensitive because of their relative large stiffness. In the United States [5], components are classified as either rigid or flexible based on their horizontal fundamental period, where NSCs with a period $T_s < 0.06\,\mathrm{s}$ are denoted as rigid. Hence, flexible NSCs are susceptible to experiencing significant amplification of acceleration responses with respect to ground. In the specific case of vertical floor motions, and based on the study presented in [4], the flexibility of the girder/slab plays an important role. The acceleration of NSCs located on open bays could be up to four times as larger as the vertical acceleration demands experienced by NSCs located close to columns.

Design forces for nonstructural components due to vertical base excitation are proposed in U.S. standards [1, 2]. In contrast, the European standard [3] does not provide explicit information on design vertical component accelerations or forces. In the United States, the recommended design component forces in the vertical direction $F_{p,v}$ are simply 50 % of the product of the design horizontal peak ground acceleration PGA_h times the seismic active mass in the vertical direction:

$$F_{p,v} = \pm 0.20\, S_{DS} W_p = \pm 0.50\, PGA_h W_p \tag{1.1}$$

Where S_{DS} is the design horizontal spectral acceleration in the short period region and W_p is the mass of the component.

In contrast to the definition in [1] we use in this study the subscripts v and h in order to clearly define the difference between horizontal and vertical direction. However, this simplified estimation is questionable since the proposed equation for vertical component forces is not based on rigorous analyses or reliable experience data. One of the main problems is the lack of recorded vertical responses from buildings due to general unavailability of buildings instrumented with accelerometers able to record vertical motions. Thus, there is the need to quantify peak vertical floor acceleration demands (PFA_v) and their associated vertical floor response spectra and propose simplified design equations. In order to accomplish the aforementioned objectives, this study is divided into the following sections:

- Ground motion record selection (special attention is placed on the location of the accelerometers and the corner frequencies used for signal processing and filtering).
- Quantification of vertical fundamental frequencies and corresponding mode shapes with respect to the number of stories and column-stiffness-distribution over the height of steel buildings designed based on modern codes in the United States.
- Simplified estimation of vertical peak floor acceleration demands $PFA_v^{(col)}$ for components located close to columns using generic stick models (Instead of $PFA_v^{(col)}$ - the abbreviation PFA_v is used from here on since this report focuses on vertical acceleration demands at floor locations close to columns. The counterpart to $PFA_v^{(col)}$ is the peak floor acceleration demand in vertical direction located e.g., in the middle of a girder or a slab, referred as $PFA_v^{(bay)}$. This study solely focuses on the quantification $PFA_v^{(col)}$ demand).
- Summary, conclusions, and future work on the study of vertical PFA demands.

2 Ground motion record selection

Any ground motion record selection approach based on seismic hazard information necessitates the availability of vertical pseudo-spectral acceleration spectra $\left(S_{a,v}\left(T,\zeta\right)\right)$. Unfortunately, probabilistic seismic hazard information is only available for the horizontal component of ground motion. Campbell and Bozorgnia [6, 7] developed a procedure to address this challenge without having to conduct a full-blown probabilistic seismic hazard analysis for the vertical component of ground motion. The first step involves converting the $\zeta = 5\,\%$ damped horizontal spectral acceleration at a period of $0.20\,\mathrm{s}$ $S_{a,h}\left(T = 0.20\,\mathrm{s},\zeta\right)$ to vertical spectral accelerations using vertical-to-horizontal (V/H) acceleration ratios for the site class BC boundary [8]. These ratios were estimated based on a study that involves near-source strong ground motions [6]. The second step entails the estimation of vertical spectral ordinates at all periods based on the vertical spectral ordinate at $T = 0.10\,\mathrm{s}$, modified for appropriate site conditions.

As part of the National Earthquake Hazards Reduction Program (NEHRP) in the U.S., a $\zeta = 5\,\%$ damped design vertical acceleration spectrum was proposed in [8]. The design vertical acceleration spectrum is based on modifications made to the procedure proposed by Campbell and Bozorgnia [7]. The primary modification involved estimating design vertical spectral accelerations from horizontal spectral acceleration values which are available in seismic design maps [9]. These seismic design maps were obtained from hazard analysis using ground motion records that are part of the NGA ground motion database [10], which is the database used in this study to select ground motion records. A modified conversion factor is introduced in [8] to transform design horizontal to design vertical spectral accelerations for all soil conditions. In this process, estimates of design horizontal spectral accelerations are obtained from the $\mathrm{MCE_R}$ (risk-targeted Maximum Considered Earthquake) horizontal spectral acceleration at a period of $T = 0.20\,\mathrm{s}$ (S_S) [1]. These $\mathrm{MCE_R}$ values are provided in seismic design maps. Once this modified conversion is applied, limits are set on the design vertical spectral accelerations and ordinates at periods other than $0.10\,\mathrm{s}$ are estimated based on relationships that are a function of the period in the vertical direction [8]. This transformation is possible primarily because for most soil conditions, as well as for magnitudes (> 6.5) and distances ($< 60\,\mathrm{km}$) of interest for engineered structures, the (V/H) ratio $S_{a,v}\left(T = 0.10\,\mathrm{s},\zeta\right)/S_{a,h}\left(T = 0.20\,\mathrm{s},\zeta\right) \approx 0.80$ [8].

The approach described above leads to the vertical response spectrum in [8] (from here on referred to in this report as NEHRP-spectrum). Vertical periods (T_v) of typical civil engineering structures are much shorter than typical horizontal periods (T_h), this issue is further discussed in Section 3.3.1. Therefore, the NEHRP-spectrum is presented herein in the frequency domain. Figure 2.1 shows the normalized vertical spectral ordinate over the vertical frequency in Hz, $f_v = 1/T_v$. Spectral ordinates are normalized by the acceleration due to gravity g and $C_V S_{DS}$. Where C_V can be obtained from Table 2.1 and S_{DS} is the design horizontal spectral acceleration at short periods according to [1, 8]. The normalized NEHRP-spectrum can be constructed via the evaluation of:

$$\frac{S_{a,v}(f_v,\zeta)}{g\,C_V S_{DS}} = \begin{cases} 0.3 & \text{if } f_v \geq 40\,\text{Hz} \\ 2.0\,(1/f_v - 1/40) + 0.3 & \text{if } 20\,\text{Hz} \leq f_v \leq 40\,\text{Hz} \\ 0.8 & \text{if } 20/3\,\text{Hz} \leq f_v \leq 20\,\text{Hz} \\ 0.8\,(20/3\,f_v)^{3/4} & \text{if } 0\,\text{Hz} \leq f_v \leq 20/3\,\text{Hz} \end{cases} \tag{2.1}$$

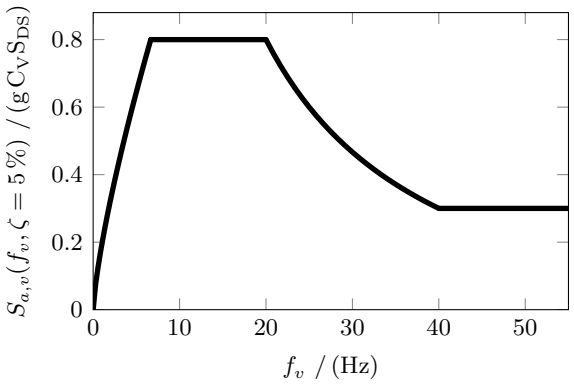

Figure 2.1: Normalized vertical design response spectrum (NEHRP-spectrum).

S_S	C_V NEHRP Site Class		
	A, B	C	D, E, F
≥ 2.00	0.90	1.30	1.50
1.00	0.90	1.10	1.30
0.60	0.90	1.00	1.10
0.30	0.80	0.80	0.90
≤ 0.20	0.70	0.70	0.70

Table 2.1: Conversation factor C_V for different site classifications.

2.1 Selection of ground motions for compatibility with the NEHRP-spectrum

In order to perform a response history analysis (RHA), at least one base-acceleration series representative of local site conditions is required. Currently, a consensus on how to select ground motions for RHA is nonexistent. However, an approach that is widely accepted and used in the earthquake engineering community is the use of base accelerations whose spectral ordinates over a desired frequency range are consistent with a target spectrum that is representative of the site. In general, this target spectrum can be obtained from either seismic hazard analysis (e.g. a design response spectrum) or a scenario analysis (e.g., from a ground motion prediction equation, GMPE). A more comprehensive discussion regarding ground motion selection methods as well as their pros and cons can be found in [11].

The ground motion record selection in this report is based on the NEHRP-spectrum, more specifically, on its spectral shape. Equation (2.1) shows that the regions of constant acceleration are independent of site conditions. In other words, the corner frequencies are constant (in contrast to those present in NEHRP design horizontal spectra). Therefore, this property of the vertical NEHRP-spectrum facilitates in part the selection of ground motion records from the NGA (PEER) ground motion database [12] based on how consistent they are either individually or as set with the spectral shape of the NEHRP-spectrum. Thus, two methods are implemented. The first method involves the selection of spectrum-compatible ground motion records while the second one involves the selection of spectrum-compatible ground motions sets. The first method is more geared toward conducting RHA to estimate central values (e.g. median) of seismic demands. The second method explicitly accounts for the record-to-record variability in the estimation of seismic demands, and hence, provides the means to evaluate seismic demands statistically.

Finding spectrum-compatible ground motion records is a computational expensive procedure. Thus, the 3181 earthquake recordings provided by the NGA (PEER) ground motion database were evaluated and a subset of recordings pre-selected based on the following characteristics:

- Moment magnitude: $M_W \geq 5.50$.
- NEHRP Site Classification D (stiff soil, shear wave velocity: $180\,\mathrm{m/s} \leq v_{s30} \leq 360\,\mathrm{m/s}$).
- Fault mechanism (FM): strike-slip (SS), reverse (RV), reverse-oblique (RVO).
- Distance (as defined by Joyner and Boore [13]): $0\,\mathrm{km} \leq r_{jb} \leq 30\,\mathrm{km}$.

A comprehensive overview of the characterization of ground motions (magnitude, fault mechanism, source to site distance, etc.) can be found in [14].

2.2 Spectrum-compatible single records

This section deals with the selection of single records that are compatible with the NEHRP-spectrum. The procedure adopted in this study to select a spectrum compatible record is based on a minimization algorithm implemented in Matlab [15]. An objective function $F(\alpha)$ is used, which is equal to the norm of the residual between spectral ordinates of the NEHRP-spectrum $\left(S_{a,v}\left(f_v,\zeta\right)\right)$ and those of the pseudo vertical acceleration response spectrum of a single ground motion $\left(\widetilde{S}_{a,v}\left(f_v,\zeta,\alpha\right)\right)$ over a predefined frequency range and a given scale factor α:

$$F(\alpha) = \left\| S_{a,v}\left(f_v,\zeta\right) - \widetilde{S}_{a,v}\left(f_v,\zeta,\alpha\right) \right\| \longrightarrow \min \tag{2.2}$$

Equation (2.1) defines the NEHRP-spectrum normalized to $C_V S_{DS}$. In order to constitute a record set independent of site conditions the product of the conversation factor and the spectral acceleration at short periods was set to $C_V S_{DS} = 1.00\,\mathrm{g}$ for the optimization procedure. The physical interpretation of the objective function is simply the spectrum-matching criterion. Typical civil engineering structures are relatively stiff in the vertical direction (see Section 3.3.1). Hence, the low frequency region is not of primary interest in this study. This allows constraining the objective function to a lower frequency value, chosen in this study to be $f_{v,low} = {}^{10}/_{3}\,\mathrm{Hz}$. A reasonable upper limit of the frequency range is the corner frequency at which the PGA_v

becomes constant at $f_{v,up} = 40\,\text{Hz}$ (see Figure 2.1). This upper limit is deemed to be reasonable given that it is consistent with the definition of the zero-period nonstructural component (NSC) in the ICC-ES acceleration spectrum used for seismic qualification by shake table testing of NSC [5]. In this document, the zero-period NSC is defined at frequencies $f \geq 100/3\,\text{Hz}$, thus, $f_{v,up} = 40\,\text{Hz}$ is a representative upper limit to evaluate the objective function. Using the proposed limits for evaluation of the objective function leads to records that can be used for assessment of peak vertical floor acceleration demands as well as for estimation of vertical floor response spectra.

The scale factor α for a single record was modified during the optimization approach until the objective function was minimized. In order to accelerate the optimization process and to avoid unreasonable values for scale factors, the boundaries of α were set to:

$$1/5 \leq \alpha \leq 5 \tag{2.3}$$

This approach may appear to be arbitrary; however, this range of scale factors was used since a study of Heo, Kunnath and Abrahamson [16] utilized a comparable range of scale factors of $0.61 \leq \alpha \leq 3.41$ during their ground motion selection approach.

Solving the constrained minimization problem leads to the required scale factors for each ground motion record. The records that constituted the three best matches are listed in Table 2.2.

No.	Earthquake Name	Station Name	Year	M_W	FM	r_{jb}	α
1	Whittier Narrows-01	LA - 116th St School	1987	5.99	RVO	18.23	3.62
2	Whittier Narrows-01	Covina - W Badillo	1987	5.99	RVO	9.49	3.33
3	Whittier Narrows-01	West Covina - S Orange Ave	1987	5.99	RVO	6.42	2.33

Table 2.2: Basic characteristics of best three ground motion records matching the NEHRP-spectrum.

It should be noted that if ground motions from NEHRP site classifications C and D are allowed (instead of D only), a ground motion record from the Manjil (Iran) earthquake results as the optimum one.

Figure 2.2a shows the single record spectra and the NEHRP-spectrum for $C_V S_{DS} = 1.00$. The vertical grid lines show the boundaries for evaluation of the objective function. In order to quantify the accuracy of spectral ordinates of these records with respect to the NEHRP-spectrum, the relative error is determined by evaluation of:

$$err^{(rel)} = \frac{S_{a,v}(f_v, \zeta, \alpha) - S_{a,v}(f_v, \zeta)}{S_{a,v}(f_v, \zeta)}\,100 \tag{2.4}$$

Positive values of $err^{(rel)}$ indicate an overestimation. From Figure 2.2b it can be seen that each record matches the NEHRP-spectrum with adequate accuracy. This is particularly true for the frequency band used to evaluate the objective function, which is also represented by vertical grid lines in Figure 2.2b. It is evident that the average of the relative error is approximately equal to zero. In the low frequency region, $f < 10/3\,\text{Hz}$, the relative error tends to grow very rapidly because the spectral acceleration values in the denominator of Equation (2.4) tend to zero as the frequency approaches zero.

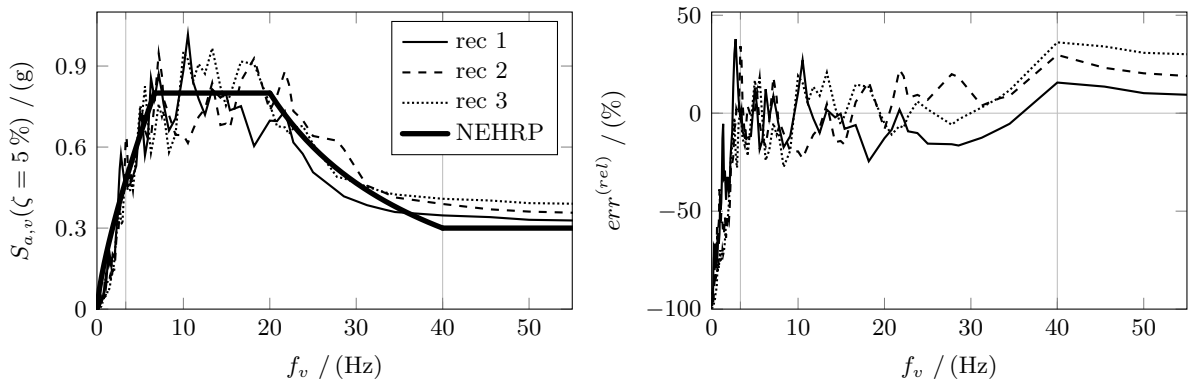

(a) (b)

Figure 2.2: (a) Spectra of three best spectrum-compatible ground motion records and (b) relative error with respect to the NEHRP spectral ordinates .

2.3 Spectrum-compatible record sets

In order to evaluate seismic demands statistically, a set of records is required to account for the record-to-record variability. Thus, the second ground motion selection method used in this study is based on a group of records from the NGA (PEER) ground motion database in which the same scale factor α is applied to each record according to the following criteria:

- The median spectral acceleration for the set $\widetilde{S}_{a,v}(f_v, \zeta, \alpha)$ should match the normalized NEHRP-spectrum over the frequency range of interest.
- The dispersion, which is measured as the standard deviation of the natural logarithm of the values for a given frequency, $\sigma_{S_{a,v}(f_v,\zeta,\alpha)}$ should be equal to a predefined target dispersion $\sigma_t(f_v) = \sigma_t$.

These two targets constitute two different spectrum-matching requirements. This leads to two coupled objective functions that can be minimized using genetic algorithms implemented in Matlab [15] for multicomponent objective functions (again, in the definition of the NEHRP-spectrum $C_V S_{DS}$ was set to unity for the optimization procedure):

$$\left.\begin{aligned} F_1(\alpha) &= \left\| S_{a,v}(f_v, \zeta) - \widetilde{S}_{a,v}(f_v, \zeta, \alpha) \right\| \\ F_2(\alpha) &= \left\| \mathrm{e}^{\sigma_t} S_{a,v}(f_v, \zeta) - S_{84,a,v}(f_v, \zeta, \alpha) \right\| \end{aligned}\right\} \longrightarrow \min \tag{2.5}$$

In this process, spectral accelerations for a given frequency are assumed to be log-normally distributed, which is typical for response quantities in earthquake engineering [17]. Therefore, 84th percentile values $S_{84,a,v}(f_v, \zeta, \alpha)$ can be estimated by the product of the parameter e^{σ_t} and the median spectral acceleration. This forms the basis for the second component of Equation (2.5). The implementation of this approach for ground motion selection can be interpreted as semi-probabilistic since the choice of σ_t biases the record selection. However, a variation of the target dispersion of $\sigma_t = 0.4\,\mathrm{g}$, $0.6\,\mathrm{g}$, $0.8\,\mathrm{g}$ and $1.0\,\mathrm{g}$ is used to quantify this influence. This range of values is reasonable and in agreement with the range of dispersions depicted in the spectra of [18].

The solutions of the multi-objective optimization can be graphically interpreted as a Pareto-optimal solution [19], sometimes referred to as Pareto frontier. Possible realizations (i.e. spectrum matching record sets) are shown in Figures 2.4 to 2.7. Figures 2.4a to 2.7a show the spectra of individual records, their statistical measures, and the NEHRP-spectrum. Figures 2.4b to 2.7b show the distribution of the records as a function of magnitude-distance ($M_W - r_{jb}$) coordinates. Table 2.3 lists the basic properties of each record set; the total number of records in each set is given in the second column.

No.	recs	σ_t	α
1	55	0.40	1.98
2	62	0.60	1.89
3	91	0.80	2.10
4	82	1.00	2.55

Table 2.3: Basic characteristics of ground motion record sets compatible with the normalized NEHRP-spectrum.

A qualitatively evaluation of the median spectrum of each ground motion set shows that each median spectrum is an adequate approximation of the target spectrum in the region $0\,\text{Hz} \leq f_v \leq {}^{20}/_{3}\,\text{Hz}$ (Figures 2.4a to 2.7a). The quality of the approximation in the region around the corner frequency $f_v = 20\,\text{Hz}$ increases with increasing number of records (not with increasing dispersion as discussed later). Furthermore, the median spectrum of each record set fits optimally the NEHRP-spectrum at the frequency of $f_v \approx 27\,\text{Hz}$ and each record set over predicts the target spectrum in the high frequency region.

The distribution of ground motions with respect to magnitude and distance for each record set is shown in Figures 2.4b to 2.7b. It is evident that most of the ground motion records belong to earthquakes with moment magnitudes between $6.0 \leq M_W \leq 6.7$, as shown in Table 2.4.

In order to define an optimal record set out of the four sets presented in Table 2.3, an understanding of the influence of the number of records and the target dispersion is required. Therefore, the relation between number of records and target dispersion is depicted in Figure 2.3, where the markers show the data listed in Table 2.3 and the solid line is a smooth interpolation polynomial.

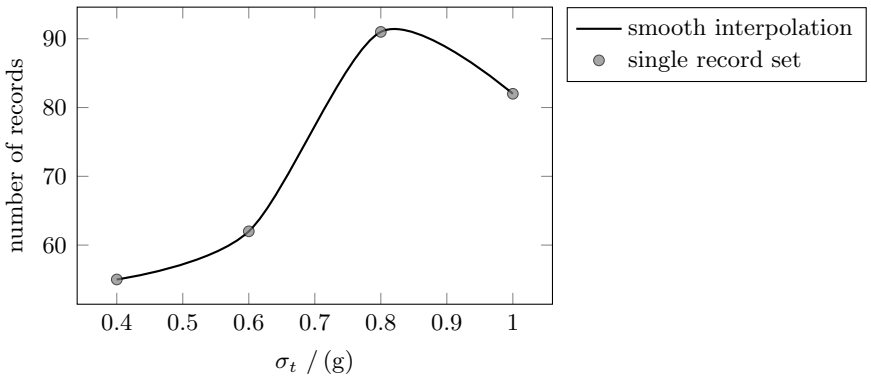

Figure 2.3: Relation between target dispersion σ_t and number of records (graphical interpretation of Table 2.3) and its smooth interpolation.

A larger number of records provides a closer and smoother approximation of the median to the NEHRP-spectrum. Moreover, when the target dispersion σ_t approaches zero, the spectrum of each ground motion record should closely match the target spectrum. This condition is only a theoretical consideration since each record has a different spectral shape. The probability density function (PDF) for this theoretical case degenerates from a log-normal distribution to the Dirac delta function. The conclusion is that competing objectives are present and, in general, increasing the number of records is required to obtain larger target dispersion values.

An optimal solution for the proposed record sets of this study can be obtained from Table 2.3 and from the graphical interpretation shown in Figure 2.3. Record set number three ($\sigma_t = 0.80\,\mathrm{g}$) consists of the maximum number of records. Comparison of the median spectrum between Figures 2.6a and 2.7a as well as a qualitative evaluation of the relative error in Figure 2.8 leads to a different conclusion than described before - record set number four shows fewer records than set number three but a median spectrum with a better compatibility with the NEHRP-spectrum. It can then be expected that a record set with a target dispersion of $0.80\,\mathrm{g} \leq \sigma_t \leq 1.00\,\mathrm{g}$ should lead to an optimal solution, i.e., a reasonable compromise between number of records, dispersion, and medium spectrum compatibility. Figure 2.3 shows that the peak value is very close to $\sigma_t = 0.80\,\mathrm{g}$, thus in this study the median of record set number three is selected as the optimal fit to the NEHRP-spectrum. From here on, in this report, this record set is referred to as the VGM record set. The basic characteristics of the single ground motion records constituting the VGM record set are listed in Table 2.4.

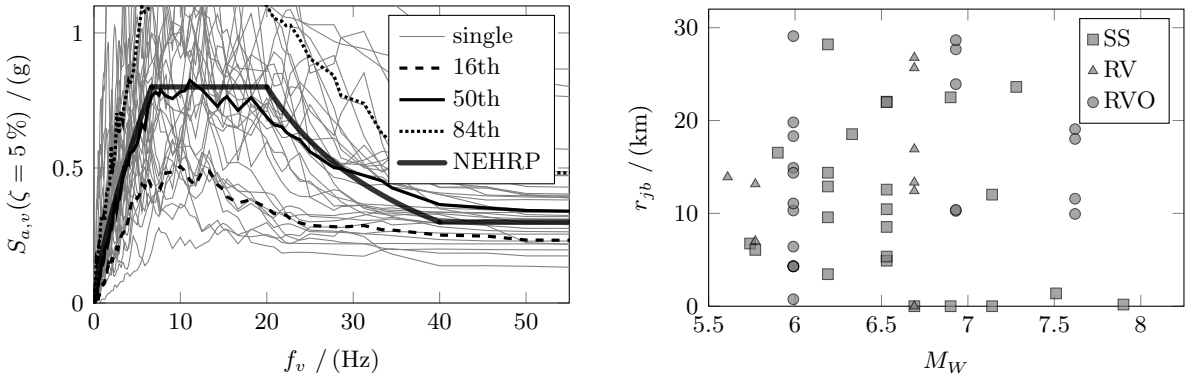

(a) (b)

Figure 2.4: (a) Spectra of ground motion record sets and (b) distribution of records compatible with the normalized NEHRP-spectrum for a given target dispersion $\sigma_t = 0.40\,\mathrm{g}$.

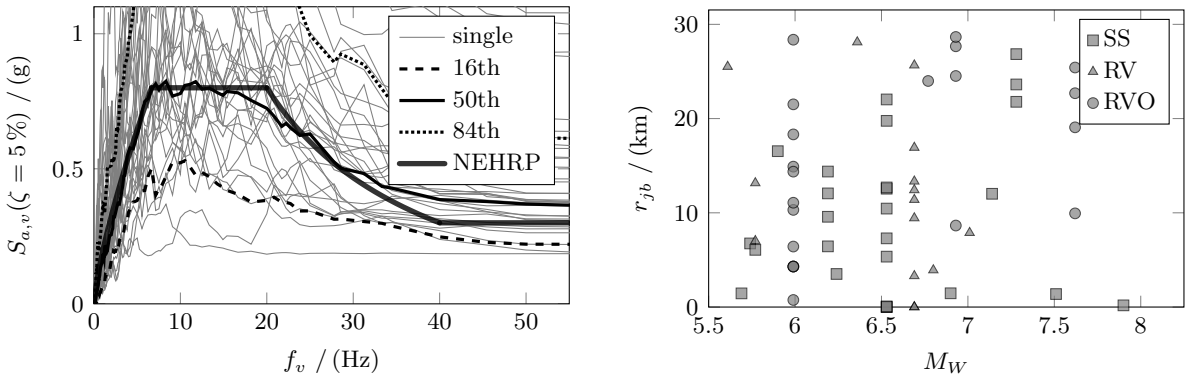

(a) (b)

Figure 2.5: (a) Spectra of ground motion record sets and (b) distribution of records compatible with the normalized NEHRP-spectrum for a given target dispersion $\sigma_t = 0.60\,\mathrm{g}$.

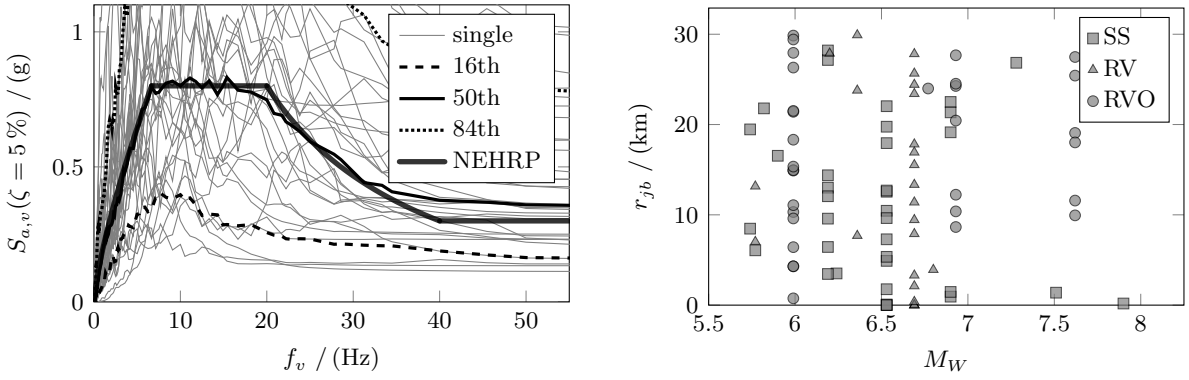

(a) (b)

Figure 2.6: (a) Spectra of ground motion record sets and (b) distribution of records compatible with the normalized NEHRP-spectrum for a given target dispersion $\sigma_t = 0.80\,\mathrm{g}$.

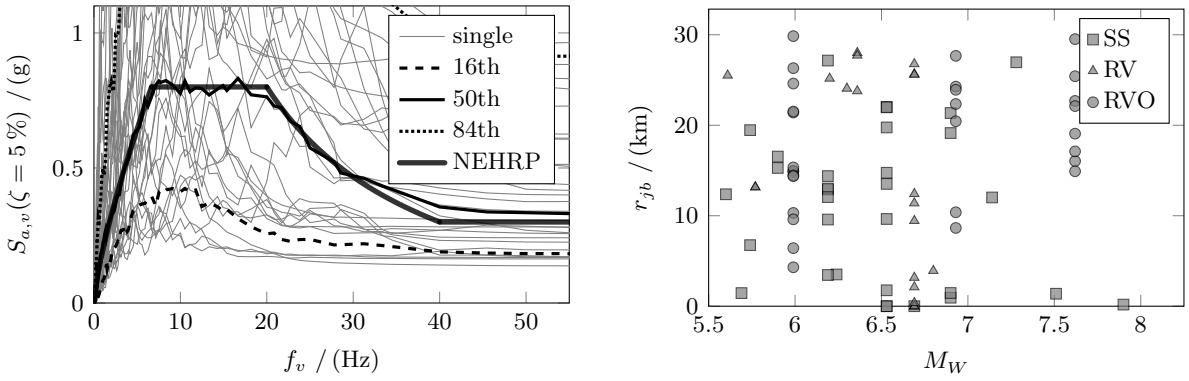

(a) (b)

Figure 2.7: (a) Spectra of ground motion record sets and (b) distribution of records compatible with the normalized NEHRP-spectrum for a given target dispersion $\sigma_t = 1.00\,\mathrm{g}$.

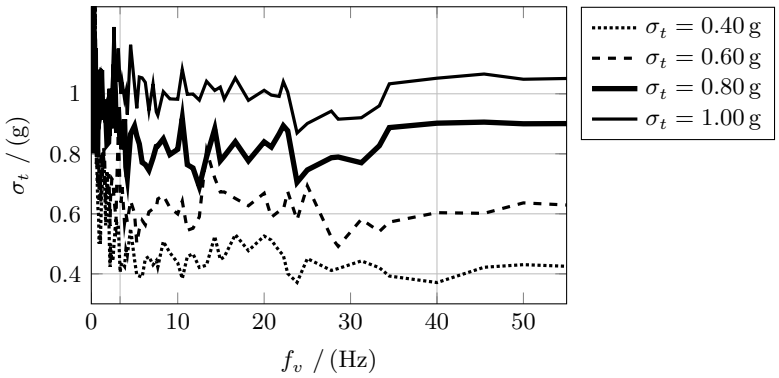

Figure 2.8: Variation with frequency of the dispersion of ground motion record sets compatible with the normalized NEHRP-spectrum for a given target dispersion.

No.	Earthquake Name	Station Name	Year	M_W	FM	r_{jb}
1	Parkfield	Cholame - Shandon Array 5	1966	6.19	SS	9.58
2	Managua, Nicaragua-01	Managua, ESSO	1972	6.24	SS	3.51
3	Gazli, USSR	Karakyr	1976	6.80	RV	3.92
4	Coyote Lake	Gilroy Array 2	1979	5.74	SS	8.47
5	Coyote Lake	San Juan Bautista, 24 Polk St	1979	5.74	SS	19.46
6	Imperial Valley-06	Aeropuerto Mexicali	1979	6.53	SS	0.00
7	Imperial Valley-06	Calexico Fire Station	1979	6.53	SS	10.45
8	Imperial Valley-06	Chihuahua	1979	6.53	SS	7.29
9	Imperial Valley-06	Delta	1979	6.53	SS	22.03
10	Imperial Valley-06	El Centro - Meloland Geot. Array	1979	6.53	SS	0.07
11	Imperial Valley-06	El Centro Array 1	1979	6.53	SS	19.76
12	Imperial Valley-06	El Centro Array 11	1979	6.53	SS	12.56
13	Imperial Valley-06	El Centro Array 12	1979	6.53	SS	17.94
14	Imperial Valley-06	El Centro Array 4	1979	6.53	SS	4.90
15	Imperial Valley-06	El Centro Array 5	1979	6.53	SS	1.76
16	Imperial Valley-06	El Centro Array 6	1979	6.53	SS	0.00
17	Imperial Valley-06	Holtville Post Office	1979	6.53	SS	5.35
18	Imperial Valley-06	Parachute Test Site	1979	6.53	SS	12.69
19	Imperial Valley-06	SAHOP Casa Flores	1979	6.53	SS	9.64
20	Westmorland	Parachute Test Site	1981	5.90	SS	16.54
21	Coalinga-01	Cantua Creek School	1983	6.36	RV	23.78
22	Coalinga-01	Parkfield - Fault Zone 7	1983	6.36	RV	29.91
23	Coalinga-01	Pleasant Valley P.P. - yard	1983	6.36	RV	7.69
24	Coalinga-05	Coalinga-14th Elm (Old CHP)	1983	5.77	RV	7.02
25	Coalinga-05	Pleasant Valley P.P. - yard	1983	5.77	RV	13.16
26	Morgan Hill	Gilroy Array 3	1984	6.19	SS	13.01
27	Morgan Hill	Gilroy Array 7	1984	6.19	SS	12.06
28	Morgan Hill	Halls Valley	1984	6.19	SS	3.45
29	Morgan Hill	San Juan Bautista, 24 Polk St	1984	6.19	SS	27.15
30	Bishop (Rnd Val)	McGee Creek - Surface	1984	5.82	SS	21.79
31	Chalfant Valley-01	Zack Brothers Ranch	1986	5.77	SS	6.07
32	Chalfant Valley-02	Bishop - LADWP South St	1986	6.19	SS	14.38
33	Chalfant Valley-02	McGee Creek - Surface	1986	6.19	SS	28.20
34	Chalfant Valley-02	Zack Brothers Ranch	1986	6.19	SS	6.44
35	Whittier Narrows-01	Bell Gardens - Jaboneria	1987	5.99	RVO	10.31
36	Whittier Narrows-01	Carson - Catskill Ave	1987	5.99	RVO	29.85
37	Whittier Narrows-01	Compton - Castlegate St	1987	5.99	RVO	18.32
38	Whittier Narrows-01	Downey - Birchdale	1987	5.99	RVO	14.90
39	Whittier Narrows-01	Downey - Co Maint Bldg	1987	5.99	RVO	14.95
40	Whittier Narrows-01	El Monte - Fairview Av	1987	5.99	RVO	0.75
41	Whittier Narrows-01	Hacienda Heights - Colima	1987	5.99	RVO	9.60
42	Whittier Narrows-01	Inglewood - Union Oil	1987	5.99	RVO	21.41
43	Whittier Narrows-01	LA - Baldwin Hills	1987	5.99	RVO	21.51
44	Whittier Narrows-01	LA - Fletcher Dr	1987	5.99	RVO	11.07
45	Whittier Narrows-01	LA - N Faring Rd	1987	5.99	RVO	27.94
46	Whittier Narrows-01	LA - N Westmoreland	1987	5.99	RVO	15.34
47	Whittier Narrows-01	Lawndale - Osage Ave	1987	5.99	RVO	26.31
48	Whittier Narrows-01	Pasadena - Brown Gym	1987	5.99	RVO	4.30
49	Whittier Narrows-01	Pasadena - CIT Calif Blvd	1987	5.99	RVO	4.30
50	Whittier Narrows-01	Playa Del Rey - Saran	1987	5.99	RVO	29.42

Continued on next page

No.	Earthquake Name	Station Name	Year	M_W	FM	r_{jb}
51	Whittier Narrows-01	West Covina - S Orange Ave	1987	5.99	RVO	6.42
52	Spitak, Armenia	Gukasian	1988	6.77	RVO	23.99
53	Loma Prieta	Agnews State Hospital	1989	6.93	RVO	24.27
54	Loma Prieta	Capitola	1989	6.93	RVO	8.65
55	Loma Prieta	Coyote Lake Dam (Downst)	1989	6.93	RVO	20.44
56	Loma Prieta	Gilroy Array 2	1989	6.93	RVO	10.38
57	Loma Prieta	Gilroy Array 3	1989	6.93	RVO	12.23
58	Loma Prieta	Hollister - South Pine	1989	6.93	RVO	27.67
59	Loma Prieta	Hollister Differential Array	1989	6.93	RVO	24.52
60	Landers	North Palm Springs	1992	7.28	SS	26.84
61	Northridge-01	Arleta - Nordhoff Fire Sta	1994	6.69	RV	3.30
62	Northridge-01	Beverly Hills - 14145 Mulhol	1994	6.69	RV	9.44
63	Northridge-01	Canoga Park - Topanga Can	1994	6.69	RV	0.00
64	Northridge-01	Canyon Country - W Lost Cany	1994	6.69	RV	11.39
65	Northridge-01	Hollywood - Willoughby Ave	1994	6.69	RV	17.82
66	Northridge-01	LA - Century City CC North	1994	6.69	RV	15.53
67	Northridge-01	LA - Fletcher Dr	1994	6.69	RV	25.66
68	Northridge-01	LA - N Westmoreland	1994	6.69	RV	23.40
69	Northridge-01	LA - Pico Sentous	1994	6.69	RV	27.82
70	Northridge-01	Moorpark - Fire Sta	1994	6.69	RV	16.92
71	Northridge-01	N Hollywood - Coldwater Can	1994	6.69	RV	7.89
72	Northridge-01	Newhall - W Pico Canyon Rd.	1994	6.69	RV	2.11
73	Northridge-01	Pacific Palisades - Sunset	1994	6.69	RV	13.34
74	Northridge-01	Playa Del Rey - Saran	1994	6.69	RV	24.42
75	Northridge-01	Rinaldi Receiving Sta	1994	6.69	RV	0.00
76	Northridge-01	Sylmar - Converter Sta	1994	6.69	RV	0.00
77	Northridge-01	Tarzana - Cedar Hill A	1994	6.69	RV	0.37
78	Kobe, Japan	KJMA	1995	6.90	SS	0.94
79	Kobe, Japan	Kakogawa	1995	6.90	SS	22.50
80	Kobe, Japan	OSAJ	1995	6.90	SS	21.35
81	Kobe, Japan	Shin-Osaka	1995	6.90	SS	19.14
82	Kobe, Japan	Takatori	1995	6.90	SS	1.46
83	Kocaeli, Turkey	Yarimca	1999	7.51	SS	1.38
84	Chi-Chi, Taiwan	CHY025	1999	7.62	RVO	19.07
85	Chi-Chi, Taiwan	CHY101	1999	7.62	RVO	9.94
86	Chi-Chi, Taiwan	CHY104	1999	7.62	RVO	18.02
87	Chi-Chi, Taiwan	TCU038	1999	7.62	RVO	25.42
88	Chi-Chi, Taiwan	TCU110	1999	7.62	RVO	11.58
89	Chi-Chi, Taiwan	TCU112	1999	7.62	RVO	27.48
90	Denali, Alaska	TAPS Pump Station 10	2002	7.90	SS	0.18
91	Chi-Chi, Taiwan-03	CHY025	1999	6.20	RV	27.88

Table 2.4: Basic characteristics of ground motion records constituting the VGM record set ($\sigma_t = 0.80\,\mathrm{g}$, $\alpha = 2.10$) compatible with the normalized NEHRP-spectrum.

3 Study of modal properties of perimeter frames of real steel frame structures

The objective of this section is to generate models of steel moment-resisting frame buildings designed based on older and modern United States codes to attain much needed information on the quantification of modal properties in the vertical direction. In order to accomplish this objective, the three Los Angeles structures designed based on the UBC 94 [20] as part of the SAC steel project [4, 21], as well as six archetype buildings designed based on IBC 2009 [22], as part of the ATC-76-1 project [23] are modeled using SAP2000 [24]. Two-dimensional models were separated into moment resisting frames and gravity frames. As a departure point, the structures of the perimeter (moment-resisting) frames are modeled and modal properties in the lateral direction are compared with results from the literature [4, 21, 23] to ensure quality of modeling. The second step deals with analysis of the models in the vertical direction. Then, a discussion of the results and the their statistical evaluation are also presented.

3.1 Perimeter frames of the SAC steel project

3.1.1 Structural models and quantification of modal periods and mode shapes in the lateral direction

The first set of frames used in this study corresponds to those from the SAC steel project in which moment-resisting frames where designed for three seismic-hazard regions in the U.S.: Los Angeles, Seattle, and Boston [21]. In this research, the three pre-Northridge frames for the Los Angeles region are used for the evaluation of modal properties. These frames correspond to buildings with 3, 9, and 20 stories. For simplification, centerline models are used since panel zone behavior is not a significant contributor to vertical acceleration demands.

A schematic visualization of the geometry of each moment resisting frame is given in Figure 3.1. Lumped masses are represented by circles and squares correspond to support conditions. Columns of the 3-story frame are fixed at their base, while columns of the 9- and 20-story frames are pinned. The 9- and the 20-story structure have one- and two-level basements, respectively, which are supported in the horizontal direction. Nodes at an elevation of 0 are prevented from translation in the horizontal direction as they represent ground level. The height of the first story of the 9- and 20-story frame is $h = 18\,\text{ft}$, while all upper stories have a constant height of $h = 13\,\text{ft}$. The first story height of the 3-story frame is also 13 ft. The width of the bays is $b = 30\,\text{ft}$ for the 3- and 9-story structure and $b = 20\,\text{ft}$ of the 20 story frame. Detailed information regarding geometry, properties of sections, modeling details and seismic masses can be found in [4, 21].

The first three fundamental periods for the SAC models used in this study are shown in Table 3.1. Lateral modal periods determined by Gupta and Krawinkler [21] (column referred as Gupta) and Wieser et al. [4] (column referred as Wieser) are presented for comparison. An

evaluation of the results presented in these tables demonstrates that the lateral modal periods of the models in this study are consistent with those obtained by previous researchers.

Figure 3.2 shows the fundamental mode shapes in lateral direction ϕ_{1h}. The vertical axis is the relative height h_{rel} which is defined as the ratio of the floor height from ground level to the total height of the structure above ground. As already mentioned, the 9- and 20-story frames have a basement, which is also prevented from horizontal and vertical translation at the base. Therefore, the corresponding elements of those mode shapes equal zero in Figure 3.2. However, the fundamental mode shapes in the lateral direction show a linear variation over the structure's height independent of the number of stories.

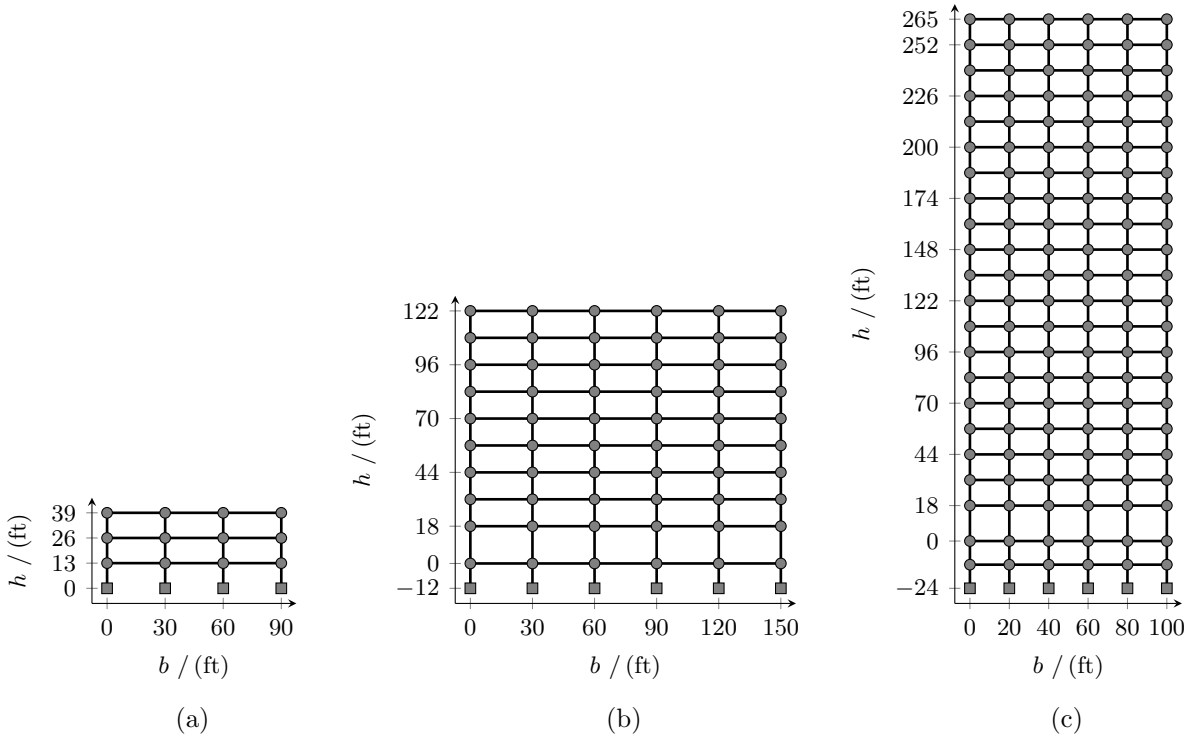

Figure 3.1: Geometry of the pre-Northridge perimeter frames from the SAC steel project. (a) 3-story frame, (b) 9-story frame and (c) 20-story frame.

period	3-stories, period / (s)			9-stories, period / (s)			20-stories, period / (s)		
No.	Study	Gupta	Wieser	Study	Gupta	Wieser	Study	Gupta	Wieser
T_{1h}	1.03	1.03	1.10	2.28	2.34	2.39	3.90	3.98	3.89
T_{2h}	0.38	0.33	0.33	0.91	0.88	0.80	1.38	1.36	1.37
T_{3h}	0.23	0.17	n.a.	0.55	0.50	n.a.	0.82	0.79	n.a.

Table 3.1: Lateral modal periods of the perimeter frames of the SAC steel project.

3.1.2 Quantification of modal periods and mode shapes in the vertical direction

The structures of the perimeter frames shown in Figure 3.1 in combination with seismic active masses in the vertical direction obtained from Table 3.2 are used for modal analysis in the

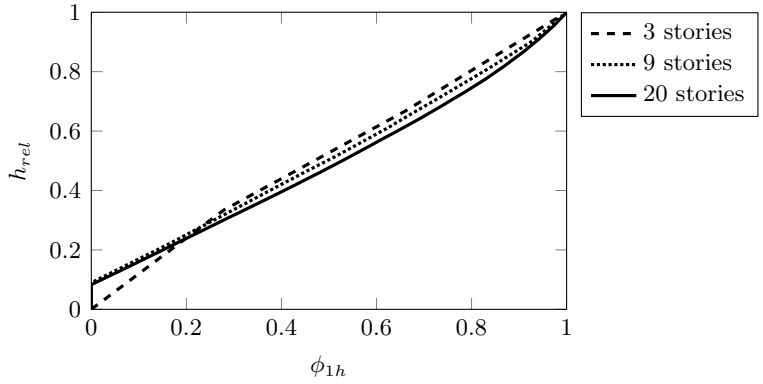

Figure 3.2: Normalized fundamental mode shapes in the lateral direction ϕ_{1h} for the perimeter frames of the SAC steel project.

vertical direction. Table 3.2 does not include the mass of structural members of the perimeter frames, for their self-weight is explicitly accounted for in the finite element analysis (FEA). Furthermore, Table 3.2 represents the masses of the interior columns. In the SAC steel project, precisely in [4, 21], the gravity systems constituting of beams and sub-beams is not defined as well as in the ATC-76-1 project [25]. Additionally, the exterior columns of the frames are located at the corners of the building. Thus, structural models assume that an exterior column supports $1/2$ times the mass of an interior column.

floor	seismic mass / (kips s^2/ft)			seismic mass / (t)		
	3-story	9-story	20-story	3-story	9-story	20-story
roof	1.30	1.28	0.59	18.90	18.68	8.56
$3 \leq$ floor $<$ roof	1.18	1.18	0.55	17.27	17.15	8.01
2	1.18	1.20	0.56	17.27	17.50	8.22

Table 3.2: Vertical seismic active mass (mass of structural members excluded) of the interior columns of the perimeter frames of the SAC steel project in U.S. customary units and SI units.

The fundamental periods T_{1v} in the vertical direction are listed in Table 3.3 and their corresponding mode shapes ϕ_{1v} are shown in Figure 3.3. Notice that the 9- and 20-story frames have approximately the same fundamental period T_{1v} probably influenced by their difference in bay widths. Comparison of the vertical fundamental periods of the SAC frames with the those of the ATC-76-1 frames is discussed in Section 3.3.1.

The normalized fundamental mode shapes in Figure 3.3 exhibit an approximate linear variation over the structure's height. A relatively small change in slope is observed at about 80% of the structure's height. This may be explained by considering that at top levels member sizes in the design tend to be controlled by gravity load demands as opposed to lateral load demands. The contrary is normally the case at the lower stories. Therefore, at upper stories the fundamental mode shape is dominated by larger design ratios of gravity load to lateral load demands, which makes the upper stories relatively stiffer than the bottom ones.

stories	T_{1v} / (s)
3	0.11
9	0.22
20	0.21

Table 3.3: Vertical fundamental periods of the perimeter frames of the SAC steel project.

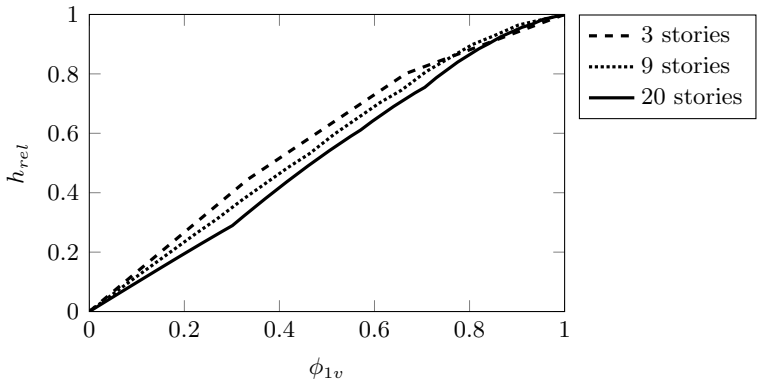

Figure 3.3: Normalized fundamental mode shapes in the vertical direction ϕ_{1v} for the first interior column of the perimeter frames of the SAC steel project.

3.2 Perimeter frames of the ATC-76-1 project

3.2.1 Structural models and quantification of modal periods and mode shapes in the lateral direction

The objective of the ATC-76-1 project was testing, refining, and applying the FEMA P-695 methodology for the quantification of building system performance and response parameters [25]. Hence, steel moment-resisting frame structures were designed as part of this project using modern design codes in the United States, where design lateral loads were determined by [26], and the structural design and detail engineering was conducted according to [27, 28]. The availability of such frames permits an evaluation of modal properties of structural systems that cover a range of design criteria from older (SAC project) to modern (ATC-76-1 project).

The ATC-76-1 steel moment resisting frame archetype (SMRF) structures are used in this study. The same simplifications applied to the SAC frames were used to model the SMRF structures (centerline model and no panel zones) in addition to neglecting reduced beam sections. Pilot studies conducted by the authors demonstrated that modeling the variation of cross-sectional properties around the reduced beam section areas had a negligible influence in vertical modal properties for bare frames.

The ATC-76-1 perimeter frames selected in this study are schematically depicted in Figures 3.4 and 3.5 where circles show lumped masses and squares indicate fixed supports. The height of the first story is $h = 18\,\text{ft}$ and all other stories have a height of $h = 13\,\text{ft}$. Figure 3.4 presents 1-, 2- and 4-story frames that were designed using the equivalent lateral force (ELF) procedure. Frames representing mid- and high-rise structures (8-, 12- and 20-story frames) were designed based on response spectrum analysis (RSA) (see Figure 3.5). Furthermore, all the frames used in this study were designed for to the maximum spectral acceleration D_{max}. A significant difference with respect the SAC frames is that the ATCE-76-1 SMRF frames do not have a

basement, and each bay width is $b = 20\,\text{ft}$, which is independent of the number of stories and number of interior gravity frames.

Table 3.4 shows the lateral fundamental periods for the ATCE-76-1 frame models generated in this study, as well as the fundamental periods obtained from [25]. The results differ for the 1- and 2-story frame; however, the fundamental periods of all other structures are consistent with those from the ATC-76-1 project.

Figure 3.6 shows the fundamental mode shapes in the lateral direction ϕ_{1h}. Here, we observe a linear variation over the structure's height too (compare with Figure 3.2).

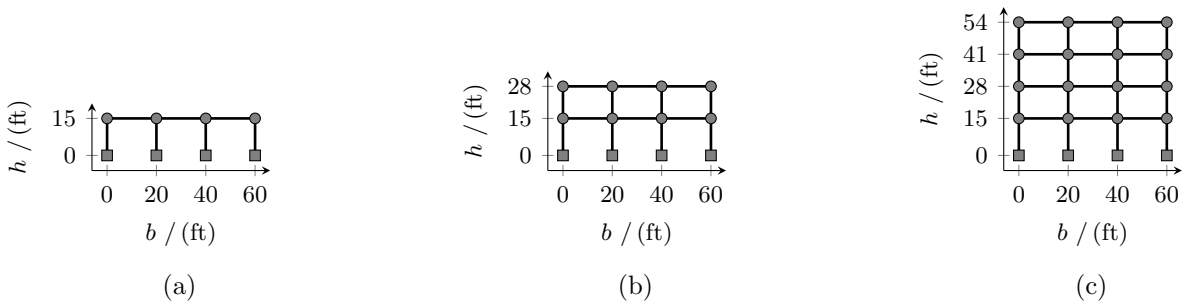

Figure 3.4: Geometry of ATC-76-1 perimeter frames. (a) 1-story frame, (b) 2-story frame and (c) 4-story frame. Design lateral loads determined by equivalent lateral force procedure.

stories	design	T_{1h}/(s) Study	ATC
1	ELF	0.42	0.71
2	ELF	0.61	0.87
4	ELF	1.27	1.30
8	RSA	2.40	2.29
12	RSA	3.26	3.12
20	RSA	4.66	4.47

Table 3.4: Lateral modal periods of the perimeter frames of the ATC-76-1 project, designed using maximum spectral acceleration D_{max}.

3.2.2 Quantification of modal periods and mode shapes in the vertical direction

Since the structural models of each perimeter frame only differ in the number of stories and the floor plans are the same for all buildings, the masses in the vertical direction defined in Table 3.5 are the same for each frame. In these models the seismic active mass of the structural frame members (i.e. columns, girders, and beams) is considered in the values listed in Table 3.5 in order to be consistent with [25].

The tributary area of the perimeter frames is defined in [25], where the exterior columns carry approximately 1.50 times the gravity load of the interior columns (excepting the mass of the cladding which is not affected by the tributary area). This difference is probably a result of the design of the gravity systems and its associated load path, e.g. how gravity loads are transferred by the gravity beams and sub-beams to the columns. Additionally, and in contrast to the SAC frames, the exterior columns of the ATC-76-1 frames are not positioned in the corners of the structure. Note, the seismic active mass of the structural members (in other

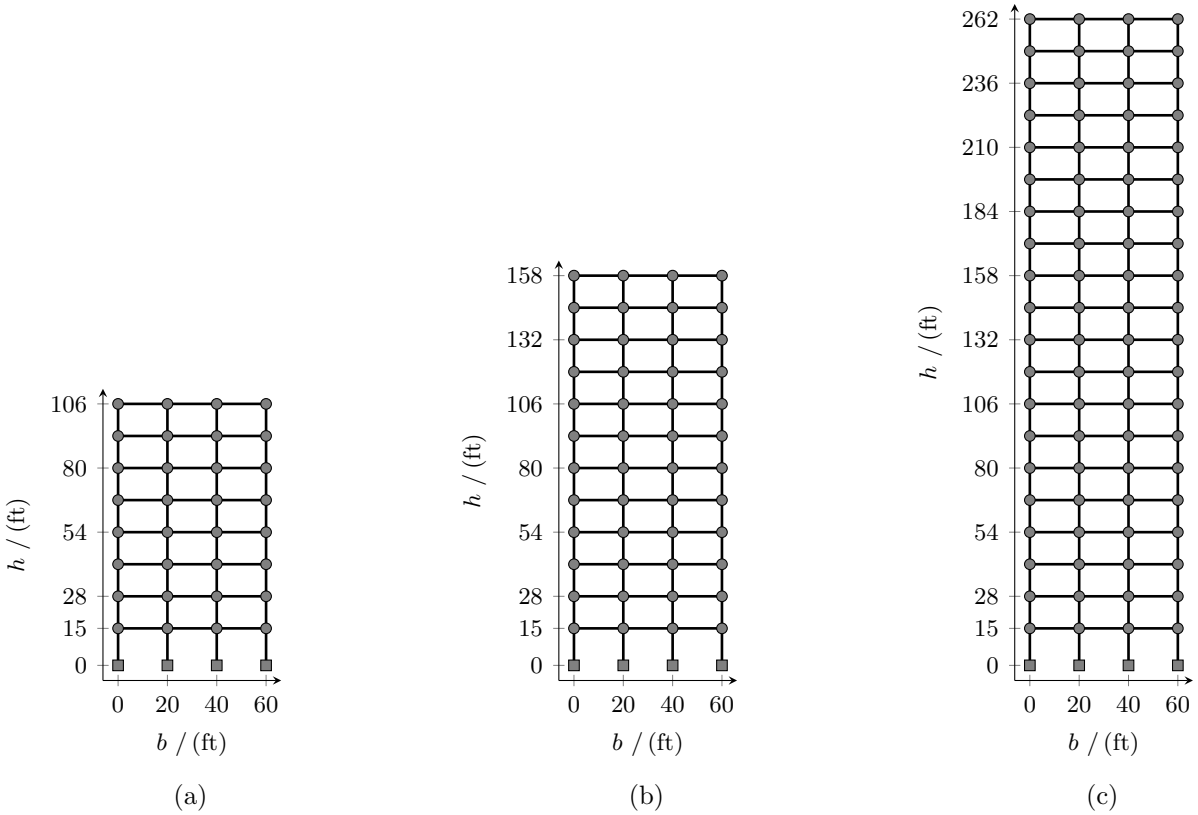

Figure 3.5: Geometry of ATC-76-1 perimeter frames. (a) 8-story frame, (b) 12-story frame and (c) 21-story frame. Design lateral loads determined by response spectrum analysis.

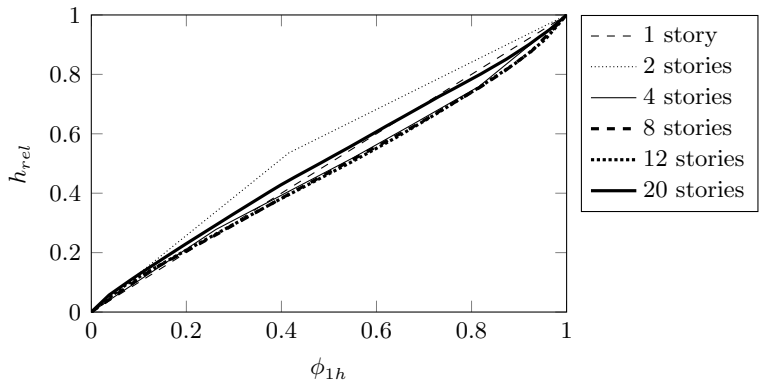

Figure 3.6: Normalized fundamental mode shapes in the lateral direction ϕ_{1h} for the perimeter frames of the ATC-76-1 project.

words the mass of columns, beams and sub-beams) is considered in the values listed in Table 3.5 in order to be consistent with [25].

Table 3.6 shows the fundamental period in the vertical direction T_{1v}. The corresponding mode shapes are shown in Figure 3.7, where a linear variation of the fundamental modal ordinate over the relative height of the structure can be observed. Similar to the SAC frames, a nonlinear branch is present between approximately 80 % of the height and the top of the structure.

floor	seismic mass/(kips s^2/ft)			seismic mass/(t)		
	exterior	interior	leaning	exterior	interior	leaning
roof	1.78	1.22	15.60	25.96	17.80	227.62
$3 \leq$ floor $<$ roof	1.88	1.32	17.21	27.43	19.27	251.20
2	1.90	1.34	17.46	27.66	19.50	254.83

Table 3.5: Vertical seismic active mass (mass of frame elements included) of the interior columns, exterior columns and leaning columns of the perimeter frames of the ATC-76-1 project in U.S. customary units and SI units.

stories	T_{1v}/(s)
1	0.03
2	0.05
4	0.10
8	0.16
12	0.20
20	0.24

Table 3.6: Vertical fundamental periods of the perimeter frames of the ATC-76-1 project.

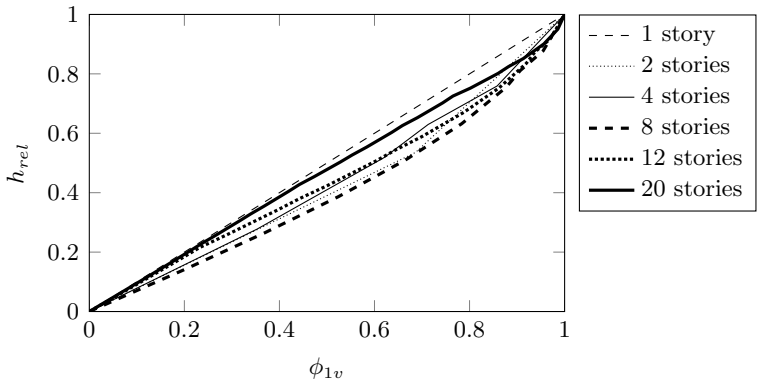

Figure 3.7: Normalized fundamental mode shapes in the vertical direction ϕ_{1v} of the interior column of the ATC-76-1 perimeter frames.

3.3 Statistical evaluation and discussion of results

3.3.1 Relation between horizontal and vertical fundamental periods

Unfortunately, no study exists to evaluate the ratio between horizontal and vertical fundamental periods of perimeter frames. Hence, Figure 3.8 shows this relation for the perimeter frames of the SAC project (squares) as well as for the ATC-76-1 project (circles). The solid line is a

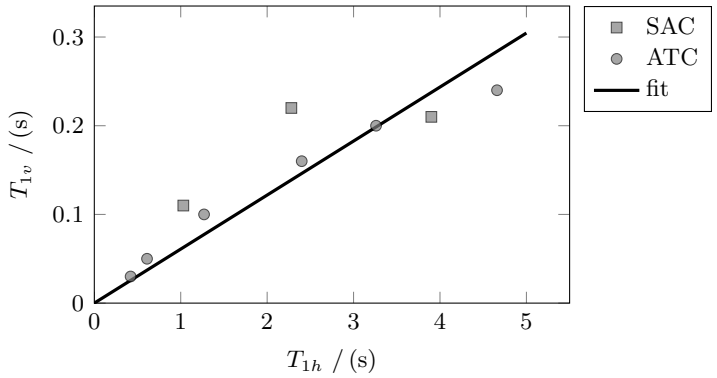

Figure 3.8: Relation between the fundamental periods in horizontal (T_{1h}) and in vertical (T_{1v}) direction for the perimeter frames of the SAC project and the ATC-76-1 project.

linear fit constrained to the origin, where it is clearly shown that the perimeter frames behave stiffer in the vertical than in the lateral direction.

$$\frac{T_{1v}}{T_{1h}} = 0.0609 \approx \frac{1}{20} \tag{3.1}$$

3.3.2 Relation between the fundamental periods and the number of stories

The primary objective of this section is to develop a relation between modal properties, in particular the fundamental period and its corresponding mode shape, and the number of stories N. These relations represent a potential basis to develop generic frame structures in order to conduct a generic evaluation of building responses in the vertical direction.

A very important modal property is the approximately linear variation of the fundamental mode shapes over the structure's height as shown in Figures 3.2, 3.3, 3.6 and 3.7 which is independent of number of stories. This structural behavior is evident and will not be discussed here in more detail.

First, the relation between number of stories and fundamental period in the lateral direction is determined. The scatter in Figure 3.9 represents the data from Tables 3.1 and 3.4. A linear variation is recognizable but when using a two-term power series the regression is more accurate, where N is the number of stories:

$$T_{1h} = 0.720N^{0.63} - 0.401 \tag{3.2}$$

Now, emphasis is placed on the relation between number of stories (or height) and fundamental period of vibration in the vertical direction. The data listed in Tables 3.3 and 3.6 for the variation of fundamental period T_{1v} with number of stories is depicted in Figure 3.10. A

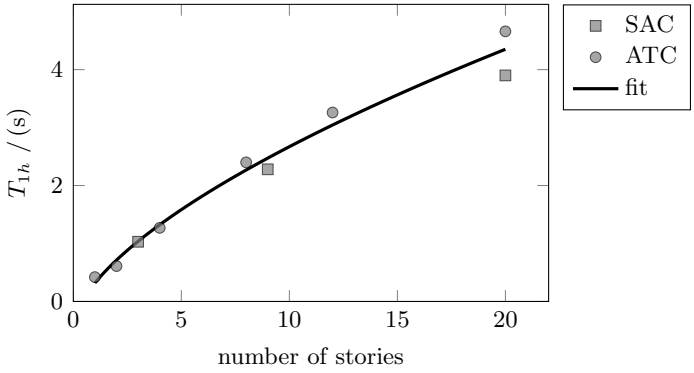

Figure 3.9: Relation between the lateral fundamental period T_{1h} and the number of stories for the SAC steel project and the ATC-76-1.

statistical regression analysis is conducted on the data shown in Figure 3.10 and again, a two-term power series is used to fit the data:

$$T_{1v} = -3.602N^{-0.02} + 3.621 \tag{3.3}$$

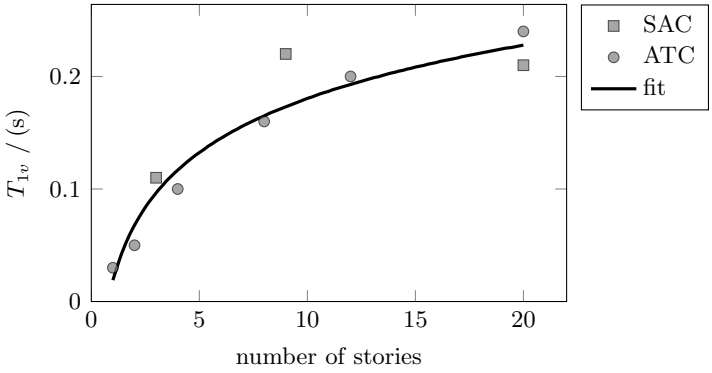

Figure 3.10: Relation between the fundamental period T_{1v} and the number of stories for the SAC steel project and the ATC-76-1 project.

The goodness of a fit can be evaluated with a scalar value in terms of the square of the correlation between the response values and the predicted response values (R^2) [15]. The closer R^2 is to one, the better is the quality of the fit. For the used two-term power laws in Equations (3.2) and (3.3) the goodness equals $R_h^2 = 0.97$ for the horizontal, respectively $R_v^2 = 0.91$ for the vertical fundamental period related to the number of stories.

Thus, Equations (3.2) and (3.3) in combination with a linear fundamental mode shape are the bases to develop generic frame models for parametric and probabilistic studies of vertical seismic demands. These generic frames will be able to reasonably represent the vibration response in both the vertical and horizontal directions.

4 Development of generic perimeter frame structures

Generic perimeter frame structures are developed in this chapter based on the information contained in Chapter 3. The properties of the SAC- and ATC-76-1 perimeter frames used to design these generic models are summarized next:

- The fundamental mode shapes are assumed to be linear with respect to the number of stories. This property holds for both the lateral and vertical directions and can be justified based on Figures 3.2, 3.3, 3.6 and 3.7.
- The fundamental periods in both directions can be estimated using Equations (3.2) and (3.3).
- The fundamental mode dominates the structural response. An useful indicator of the relative contribution of an individual mode to the total response of the system is the effective seismic active mass (as a fraction of the total seismic mass) listed in Tables 4.1 and 4.2. These values are presented for the fundamental modes in the horizontal (first column) and vertical directions (second column). It is evident from this information that the first mode dominates the response, for most of the effective seismic active mass ($> 80\,\%$ in most cases) can be attributed to the first mode. In lateral direction the effective seismic active mass is always bigger than in vertical direction, except for the 20-story ATC-76-1 frame.

stories	m_{1h} / (%)	m_{1v} / (%)
3	82.37	61.70
9	82.94	63.42
20	80.10	73.72

Table 4.1: First mode effective seismic active mass in the lateral (m_{1h}) and vertical (m_{1v}) directions of the perimeter frames of the SAC steel project.

stories	m_{1h} / (%)	m_{1v} / (%)
1	100.00	81.88
2	84.70	52.62
4	84.56	60.50
8	80.12	71.52
12	78.09	76.71
20	74.31	77.04

Table 4.2: First mode effective seismic active mass in the lateral (m_{1h}) and vertical (m_{1v}) directions of the perimeter frames of the ATC-76-1 project.

4.1 Generic stick model for approximation of interior columns

Typical perimeter frames consist of two exterior columns and, if required, interior columns to transfer equivalent lateral forces from the structure to the foundation. Figure 4.1a shows schematically a 6-story, 2-bay generic frame. Lumped masses are depicted as gray circles. The degrees of freedom with respect to the ground $(x_g(t), z_g(t))$ are denoted as $x_i(t)$ in the lateral direction and as $z_i(t)$ in the vertical direction, where i is the floor number. In order to study separately the behavior of exterior and interior columns a generic stick model for each column type is developed. In this context, a generic stick model represents an isolated column line of a frame as shown for the 6-story generic frame in Figure 4.1b for an interior column. In this report the development of the generic stick model of interior columns is illustrated. Furthermore, the story and the floor numbering as well as the enumeration of the seismic mass are defined in Figure 4.1b. Finally, Figure 4.1c shows the generic stick model of the interior column consisting of columns, rotational springs $c_{\theta i}$ (representing the flexural stiffness of the frame) and vertical springs c_{ui} (representing the shear stiffness of the girders and the axial stiffness of the exterior columns). An additionally rotational spring at the base $c_{\theta 0}$ is required to make sure that the fundamental mode in the lateral direction is a straight line over the structure's height and to obtain a uniform distribution of the moments of inertia over the height [29].

Furthermore, the assumptions outlined below are required for the formulation of the problem in the vertical and horizontal directions:

- PΔ effects are not included. In other words, modal quantities are based on first-order analyses. Thus, the global stiffness matrix $\mathbf{K}$ is in its initial state.
- Lumped masses as shown in Figure 4.1 are used. When modeling the structure with as a generic stick, the mass matrix $\mathbf{M}$ is a diagonal matrix for the lateral as well as the vertical degrees of freedom.
- The story height h is the same for each story and the bay width is l for each one of them (see Figure 4.1).
- Since SAC and the ATC-76-1 frames are steel frames, Young's modulus of $E = 2 \cdot 10^{11}\,\mathrm{N/m^2}$ is used.
- Columns splices are located at column mid-heights (except the columns of the first story, the splices of those members are located at mid height of the second story). Column cross

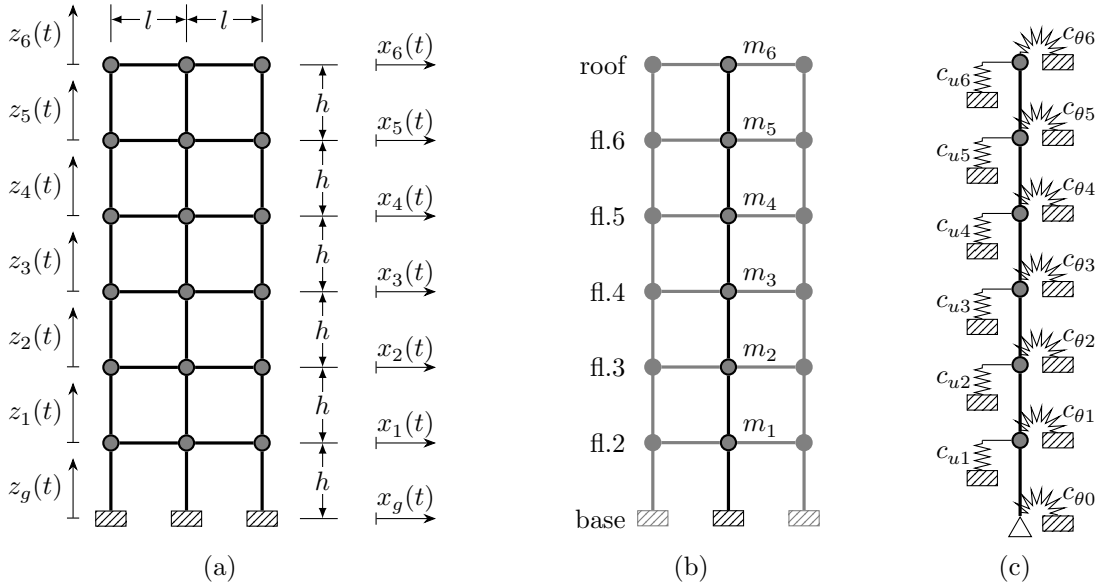

Figure 4.1: Development of generic stick models for interior columns based on a two-bay generic frame. (a) Complete generic frame, (b) isolated interior column with floor / story / mass numbering and (c) generic stick model including equivalent springs.

sectional properties vary per story and at each beam-column (BC) connection, column and girder member sizes are assumed to be the same as shown in Figure 4.2b.

4.1.1 Structural parameters in the lateral direction

In order to keep the determination of structural properties as simple as possible, it is assumed that the first mode dominates the structural response and the fundamental mode shape in the lateral direction is linear over the structure's height. The deflected shape of the frame under lateral loading assumes points of inflection (POI) at column mid-heights and beam mid-spans (Figure 4.2a). This assumption allows the use of the free-body diagram presented in Figure 4.2b by constraining the sub-structure using pinned supports at the POIs.

At each floor level, the same seismic masses $m_{ih}^{(l)}$, $m_{ih}^{(m)}$ and $m_{ih}^{(r)}$ are used at the left, mid, and right of the BC connection as shown in Figure 4.2b. Thus, the total seismic mass in the horizontal direction acting at each floor level of the perimeter frame equals:

$$m_h^{(story)} = m_{ih}^{(l)} + m_{ih}^{(m)} + m_{ih}^{(r)} \tag{4.1}$$

For this generic stick model only the mass associated with the interior column is required, therefore, $m_h = m_{ih}^{(m)}$, which implies that floor masses are constant with a value equal to that of the diagonal elements of the mass matrix $\mathbf{M}_h$ (note, the labels of the masses in Figure 4.1b don't have a subscript h to keep the figure independent of the lateral / vertical direction). The seismic mass can be easily determined from the dead load of the structure including the weight of cladding.

Equivalent lateral stiffness for the generic stick models can be obtained by imposing the deflected shape shown in Figure 4.2b to the various substructures along the height of the frame. Both exterior columns are the same. In particular each BC connection consists of a half column

of the lower story, a half column of the upper story and a half girder. In contrast, the BC connection at the interior column is stiffer since two half girders frame into it.

The stiffness of an isolated BC connection can be expressed in terms the relative lateral deformation u the bottom and top column nodes in the free-body diagram of Figure 4.2b for a unit shear load. Thus, the individual contribution of the half columns below and above the girder to the total horizontal deflection is given by:

$$u^{(col)} = \frac{(h/2)^3}{3EI_i} \tag{4.2}$$

The deflection given by Equation (4.2) is equivalent to the deformation at the tip of a cantilever column of length $h/2$ that frames into a rigid girder when a unit shear load is applied. Now, if the girder is flexible and the column is considered to be rigid in flexure, then, the relative lateral deformation between the bottom and top column nodes in the free-body diagram of Figure 4.2b for a unit shear load is given by:

$$u^{(gir,int)} = 2\frac{l/2\,(h/2)^2}{3EI_i} \tag{4.3}$$

$$u^{(gir,ext)} = 4\frac{l/2\,(h/2)^2}{3EI_i} \tag{4.4}$$

The total substructure flexibility caused by the flexibility of the columns and the girder(s) is given by:

$$u^{(int)} = 2u^{(col)} + u^{(gir,int)} \tag{4.5}$$

$$u^{(ext)} = 2u^{(col)} + u^{(gir,ext)} \tag{4.6}$$

The equivalent lateral stiffness for each column line of the substructure of Figure 4.2b is then the inverse of the flexibility given by Equations (4.5) and (4.6) and it is equal to:

$$c^{(int)} = \frac{1}{u^{(int)}} \tag{4.7}$$

$$c^{(ext)} = \frac{1}{u^{(ext)}} \tag{4.8}$$

Then, the total lateral story stiffness yields:

$$c^{(story)} = 2c^{(ext)} + c^{(int)} \tag{4.9}$$

Since the story shear force is directly proportional to the story mass (if damping is neglected), the seismic mass on the exterior columns and the interior column is proportional to the ratio between the individual joint stiffnesses and the total lateral stiffness for the substructure:

$$m_{ih}^{(m)} = \frac{c^{(int)}}{c^{(story)}} m_h^{(story)} = \frac{5}{11} m_h^{(story)} \tag{4.10}$$

$$m_{ih}^{(l)} = m_{ih}^{(r)} = \frac{c^{(ext)}}{c^{(story)}} m_h^{(story)} = \frac{3}{11} m_h^{(story)} \tag{4.11}$$

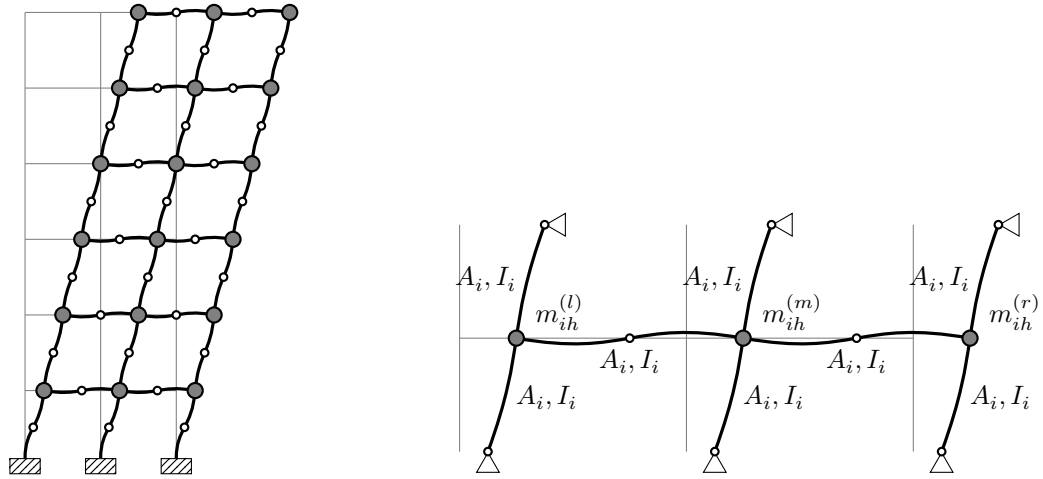

Figure 4.2: Generic frame vibrating in its lateral linear fundamental mode. (a) Complete generic frame and (b) isolated substructure.

For vibration in the lateral direction the beam members are assumed to axially rigid. Thus, the corresponding element stiffness matrix $\mathbf{K}^{(e)}$ of an beam element reads:

$$\mathbf{K}_i^{(e)} = \frac{2EI_i}{L} \begin{bmatrix} \frac{6}{L^2} & -\frac{3}{L} & \frac{6}{L^2} & -\frac{3}{L} \\ & 2 & -\frac{3}{L} & -1 \\ & & \frac{6}{L^2} & \frac{3}{L} \\ \text{symm.} & & & 2 \end{bmatrix} \tag{4.12}$$

where L is the length of the considered beam element. Again, the splices are assumed to be at the mid-height of the columns. Thus, two different stiffness matrices exist per story and per column row because the moment of inertia differs for both half column elements with respect to their location below or above the splice. The equivalent stiffness $c_{\theta i}$ of the rotational spring which represents the girders at the ith floor level (see Figure 4.2b), can be obtained by evaluation of:

$$c_{\theta i} = 2\frac{3EI_i}{l/2} = \frac{12EI_i}{l} \tag{4.13}$$

In order to obtain a uniform distribution of the moments of inertia over the structure's height a rotational spring is added at the base which *simulates* girders framed at the bottom of the first story column:

$$c_{\theta 0} = 2\frac{3EI_1}{l/2} = \frac{12EI_1}{l} \tag{4.14}$$

Assembling the global mass- and stiffness matrix using Equations (4.12) to (4.14) leads to the eigenvalue problem formulated in terms of the first eigenvalue and the corresponding linear

mode shape:

$$|\mathbf{M}_h - \lambda_{1h}\mathbf{K}_h|\,\boldsymbol{\phi}_1 = \mathbf{0} \tag{4.15}$$

where the first eigenvalue λ_{1h} (the subscript h should be the indicator for the *horizontal* direction) is the inversion of the square of the fundamental circular frequency ω_{1h}, which can be estimated by using Equation (3.2):

$$\lambda_{1h} = \frac{1}{\omega_{1h}^2} = \frac{T_{1h}^2}{4\pi^2} \tag{4.16}$$

Hence, the unknown parameters in the system of nonlinear equations in Equation (4.16) are the moments of inertia I_i; in other words there are N unknown moments of inertias if the structure is a N-story frame. Equation (4.15) can be seen as a simple optimization problem. The roots of the nonlinear system of equations can be found by the function *fsolve* which is a part of Matlab's *Optimization Toolbox* [15].

4.1.2 Structural parameters in the vertical direction

An analogous procedure to the one presented in Section 4.1.1 can be applied in the vertical direction.

For vibration in the vertical direction the seismic mass is simply defined by the associated floor tributary area. From Figure 4.3b, it can be seen that the seismic mass of the exterior column is equal to the half of the mass acting on the interior column:

$$m_{iv}^{(m)} = \frac{1}{2}m_v^{(story)} \tag{4.17}$$

$$m_{iv}^{(l)} = m_{iv}^{(r)} = \frac{1}{4}m_v^{(story)} \tag{4.18}$$

When the structure vibrates in its vertical fundamental mode (see Figure 4.3a) the vertical springs in Figure 4.1c represent the flexural stiffness of the girders. Again, the points of inflection are assumed to be located at column mid-heights and beam mid-spans as shown in Figure 4.3a. The equivalent stiffness of the vertical springs c_{ui} can be obtained from Equation (4.19), which is analogous to Equation (4.13):

$$c_{ui} = \frac{3EA_iI_i\,(h+12l)}{3I_ih^2 + A_ihl^3 + 36I_ihl + 3A_il^4} \tag{4.19}$$

Since a interior column is only loaded in its axial direction during vertical vibration, the element stiffness matrix $\mathbf{K}_i^{(e)}$ can be formulated using a truss element:

$$\mathbf{K}_i^{(e)} = \frac{EA_i}{h}\begin{bmatrix} 1 & -1 \\ -1 & 1 \end{bmatrix} \tag{4.20}$$

Finally, the eigenvalue problem formulated in terms of the linear fundamental mode shape and the corresponding eigenvalue in the vertical direction leads to:

$$|\mathbf{M}_v - \lambda_{1v}\mathbf{K}_v|\,\boldsymbol{\phi}_1 = \mathbf{0} \tag{4.21}$$

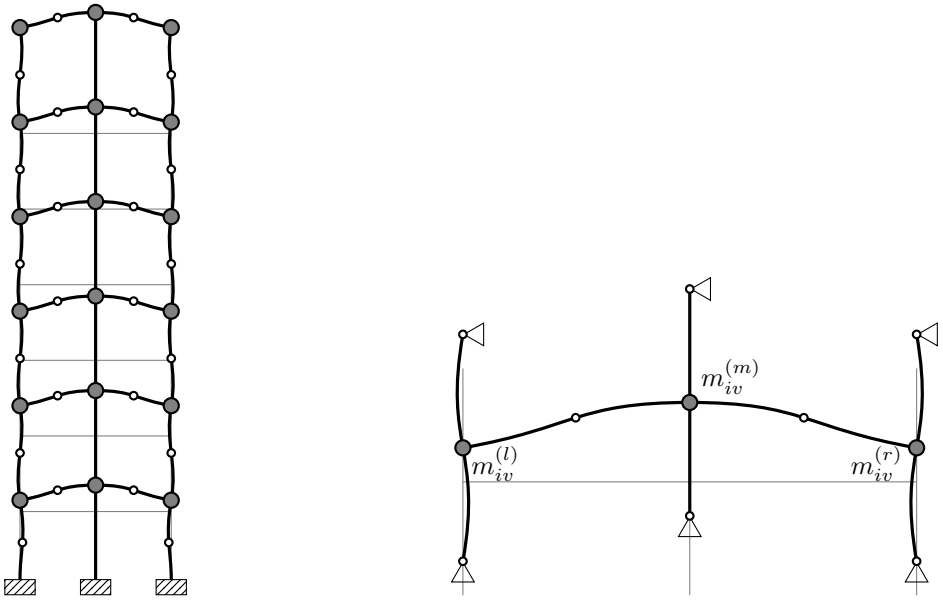

Figure 4.3: Generic frame vibrating in its vertical linear fundamental mode. (a) Complete generic frame and (b) isolated substructure.

Similar to Equation (4.16) the first eigenvalue in the vertical direction can be estimated by using Equation (3.3):

$$\lambda_{1v} = \frac{1}{\omega_{1v}^2} = \frac{T_{1v}^2}{4\pi^2} \tag{4.22}$$

The eigenvalue problem in Equation (4.21) represents the counterpart to Equation (4.15). In this case, the unknown variables are the areas A_i of the cross sections, which can determined using simple optimization techniques.

4.2 Evaluation of structural parameters

This section deals with the results from determination of the structural parameters, specifically, the moments of inertia I_i and the area A_i of the cross sections based on the approach discussed in Section 4.1. The parameters of the generic stick model is determined based on the mass and geometric characteristics outlined below:

- Seismic active story mass for vibration in the horizontal direction:

$$m_h^{(story)} = 229\,741\,\text{kg} \approx 230\,\text{t} \approx 10\,000\,\text{kip} \tag{4.23}$$

- Seismic active story mass for vibration in the vertical direction:

$$m_v^{(story)} = 19\,271\,\text{kg} \approx 19\,\text{t} \approx 830\,\text{kip} \tag{4.24}$$

- Story height, h, and bay width, l:

$$h/l = 1/2, \quad h = 3.96\,\text{m} = 13\,\text{ft} \tag{4.25}$$

Substituting Equation (4.25) into Equation (4.19) leads to a simplified formulation for the stiffness of the equivalent vertical springs:

$$c_{ui} = \frac{1}{\dfrac{7l^3}{75EI_i} + \dfrac{l}{2EA_i}} \tag{4.26}$$

Equations (4.23) and (4.24) are substituted into Equations (4.10) and (4.17) to define the seismic mass in each story in the vertical and horizontal direction.

Performing the optimization problem defined by the eigenvalue problems in Equations (4.15) and (4.21) for generic stick models with $N = 3, 6, 12,$ and 24) stories leads to the moments of inertia I_i and the area A_i of the cross sections of the generic stick.

Figure 4.4a shows the ratio between the moment of inertia of the cross section in the ith floor I_i and the cross section of the first floor I_1. The same variation of this parameter over the structure's height is applied to all generic stick models with different number of stories. The moment of inertia decreases with an increase in height. This behavior is consistent with the variation of moment of inertia found in real perimeter steel moment-resisting frames [4, 21, 25].

In contrast, the profiles of the normalized area of the cross sectional area A_i/A_1 are shown in Figure 4.4b. The 3-, 6-, and 12-story structures have distributions of cross sectional area consistent with the corresponding profiles of the moments of inertia. However, for the 24-story generic steel model, the cross sectional area grows with increasing height up to approximately $2/3\,h_{rel}$, which is not consistent with the distribution of cross sectional areas in real perimeter frames. A reasonable explanation is that the generic structure is based on results (fundamental modes and corresponding periods) of real structures. A qualitatively evaluation of the difference between the fundamental periods predicted from regression equations and their associated data points, as shown in Figures 3.9 and 3.10, leads to the conclusion that the error is larger for tall structures than for low-rise structures. This is another reason why the profile of the relative cross sectional areas of the 24-story generic stick model deviates from that of the actual structure. However, the maximum ratio is smaller than 1.10 (see Table 4.7), thus, the model is deemed to be adequate to study its dynamic behavior.

Fundamental periods, section properties, and stiffnesses of the springs of the generic stick models are listed in Table 4.3. Tables 4.4 to 4.7 list the relative stiffness ratios used to construct the complete generic stick model.

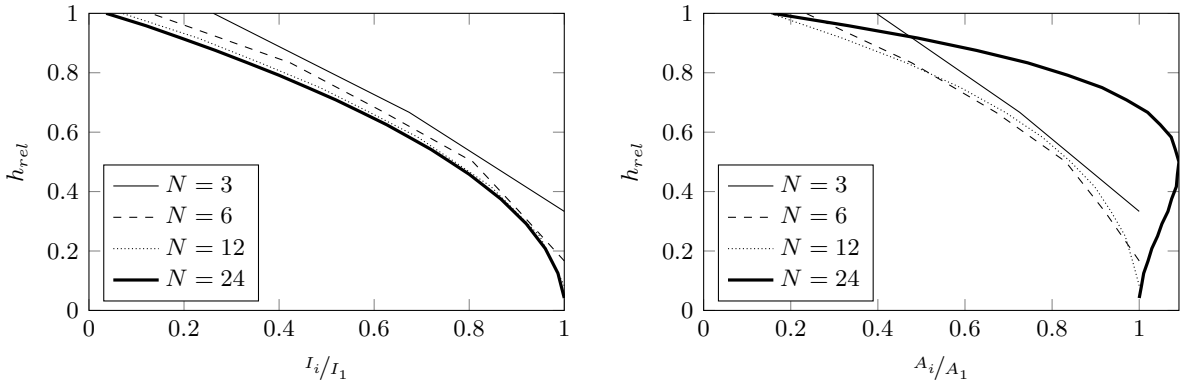

(a) (b)

Figure 4.4: Distribution of (a) the moments of inertia I_i and (b) the areas A_i of the cross sections over the relative height for the generic stick models used in this study.

stories	$T_{1h}/(\mathrm{s})$	$T_{1v}/(\mathrm{s})$	$I_1/(\mathrm{m}^4)$	$A_1/(\mathrm{m}^2)$	$c_{\theta 0}/(\mathrm{Nm/rad})$	$c_{\theta 1}/(\mathrm{Nm/rad})$	$c_{u0}/(\mathrm{N/m})$
3	1.04	0.10	$1.76 \cdot 10^{-3}$	$9.09 \cdot 10^{-3}$	$2.67 \cdot 10^{8}$	$5.33 \cdot 10^{8}$	$7.46 \cdot 10^{6}$
6	1.83	0.15	$2.01 \cdot 10^{-3}$	$1.31 \cdot 10^{-2}$	$3.05 \cdot 10^{8}$	$6.10 \cdot 10^{8}$	$8.55 \cdot 10^{6}$
12	3.04	0.19	$2.70 \cdot 10^{-3}$	$2.24 \cdot 10^{-2}$	$4.08 \cdot 10^{8}$	$8.16 \cdot 10^{8}$	$1.15 \cdot 10^{7}$
24	4.93	0.24	$3.96 \cdot 10^{-3}$	$2.77 \cdot 10^{-2}$	$5.99 \cdot 10^{8}$	$1.20 \cdot 10^{9}$	$1.68 \cdot 10^{7}$

Table 4.3: Fundamental period, section properties, and stiffness of the springs of the generic stick models.

story	h_{rel}	I_i/I_1	A_i/A_1	$c_{\theta i}/c_{\theta 1}$	c_{ui}/c_{u1}
1	0.33	1.00	1.00	1.00	1.00
2	0.67	0.67	0.73	0.67	0.67
3	1.00	0.26	0.40	0.26	0.26

Table 4.4: Ratios of section properties and spring stiffnesses for the 3-story generic stick model.

story	h_{rel}	I_i/I_1	A_i/A_1	$c_{\theta i}/c_{\theta 1}$	c_{ui}/c_{u1}
1	0.17	1.00	1.00	1.00	1.00
2	0.33	0.91	0.92	0.91	0.91
3	0.50	0.81	0.83	0.81	0.81
4	0.67	0.62	0.67	0.62	0.62
5	0.83	0.42	0.48	0.42	0.42
6	1.00	0.13	0.23	0.13	0.13

Table 4.5: Ratios of section properties and spring stiffnesses for the 6-story generic stick model.

story	h_{rel}	I_i/I_1	A_i/A_1	$c_{\theta i}/c_{\theta 1}$	c_{ui}/c_{u1}
1	0.08	1.00	1.00	1.00	1.00
2	0.17	0.97	0.98	0.97	0.97
3	0.25	0.95	0.97	0.95	0.95
4	0.33	0.90	0.94	0.90	0.90
5	0.42	0.85	0.90	0.85	0.85
6	0.50	0.77	0.84	0.77	0.77
7	0.58	0.69	0.78	0.69	0.69
8	0.67	0.59	0.69	0.59	0.59
9	0.75	0.49	0.59	0.49	0.49
10	0.83	0.36	0.47	0.36	0.36
11	0.92	0.23	0.32	0.23	0.23
12	1.00	0.07	0.15	0.07	0.07

Table 4.6: Ratios of section properties and spring stiffnesses for the 12-story generic stick model.

story	h_{rel}	I_i/I_1	A_i/A_1	$c_{\theta i}/c_{\theta 1}$	c_{ui}/c_{u1}
1	0.04	1.00	1.00	1.00	1.00
2	0.08	0.99	1.01	0.99	0.99
3	0.13	0.99	1.01	0.99	0.99
4	0.17	0.97	1.02	0.97	0.97
5	0.21	0.96	1.03	0.96	0.96
6	0.25	0.94	1.04	0.94	0.94
7	0.29	0.92	1.05	0.92	0.92
8	0.33	0.89	1.07	0.89	0.90
9	0.38	0.87	1.07	0.87	0.87
10	0.42	0.83	1.09	0.83	0.84
11	0.46	0.80	1.09	0.80	0.80
12	0.50	0.76	1.09	0.76	0.76
13	0.54	0.72	1.08	0.72	0.72
14	0.58	0.67	1.07	0.67	0.68
15	0.63	0.63	1.05	0.63	0.63
16	0.67	0.57	1.02	0.57	0.58
17	0.71	0.52	0.97	0.52	0.52
18	0.75	0.46	0.91	0.46	0.46
19	0.79	0.40	0.84	0.40	0.40
20	0.83	0.33	0.74	0.33	0.34
21	0.88	0.27	0.63	0.27	0.27
22	0.92	0.19	0.49	0.19	0.20
23	0.96	0.12	0.33	0.12	0.12
24	1.00	0.04	0.16	0.04	0.04

Table 4.7: Ratios of section properties and spring stiffnesses for the 24-story generic stick model.

5 Results from numerical analysis

This section deals with the quantification of vertical acceleration demands based on response history analyses of the generic stick models exposed to ground motions from the VGM record set.

5.1 Time history analysis

5.1.1 Profiles of the horizontal peak floor acceleration demand

Figure 5.1 shows the profiles of horizontal peak floor acceleration demands (PFA_h) normalized to the horizontal peak ground acceleration PGA_h. The gray lines are the results of records from 91 recording stations (two horizontal components per record) as defined in Table 2.4. Thus, a total of 182 profiles are shown. Bold black lines depict statistical measures (i.e. percentile values).

For elastic structures, PFA_h demands decrease with increasing number of stories (increasing fundamental period) as shown in Figure 5.1. This observation is congruent with the observation of a other research groups [30–33]. The median PFA_h profiles of all models, except in the region between the base and approximately 75 % of the height of the 24-story structure, demonstrate that the peak acceleration response is amplified in with respect to the PGA_h.

The two thin black lines (referred to the legend as WN) are the profiles corresponding to the vertical NEHRP-spectrum matching single record defined in Table 2.2 from the Whittier Narrows event. Two profiles are shown, one per horizontal component of ground motion. These records underestimate the median profile in horizontal direction. Thus, this record should not be used to estimate PFA_h demands, which is expected given that (a) the NEHRP spectrum for the vertical component of ground motion is not correlated with the design horizontal spectra used in buildings codes, (b) target spectra such as the NEHRP spectrum are not representative of the spectrum of a single ground motion record, (c) the spectrum matching was conducted only for the vertical component of ground motion. However, studies of horizontal peak floor acceleration demands can be found in [30–35].

5.1.2 Profiles of the vertical peak floor acceleration demand

Profiles of vertical peak floor acceleration demands PFA_v normalized to the vertical peak ground acceleration PGA_v due to ground motions of the VGM record set and the single record matching the NEHRP-spectrum are shown in Figure 5.2. Gray lines show profiles of single records, bold black curves indicate statistical measures, and thin black lines show profiles for the Whittier Narrows earthquake record with spectral shape compatible with the NEHRP spectrum.

In contrast to the horizontal PFA demand, it can be seen that PFA_v demands increase with the number of stories (or vertical period). The maximum average amplification occurs for all structures at the roof level and it is approximately $4PGA_v$.

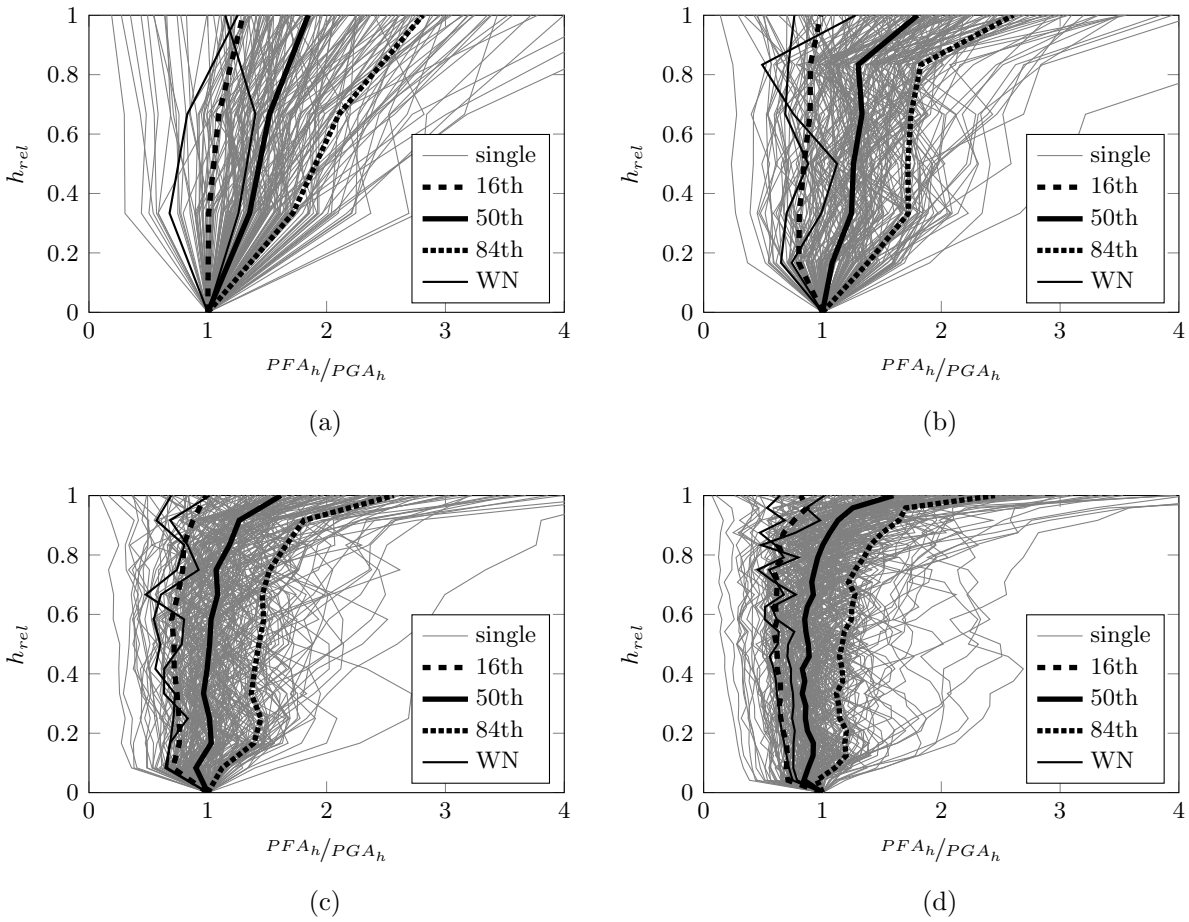

Figure 5.1: Profiles of the horizontal peak floor acceleration demand normalized to the horizontal peak ground acceleration for the (a) 3-story, (b) 6-story, (c) 12-story, and (d) 24-story generic stick models exposed to records from the VGM record set and the single record from the Whittier Narrows earthquake (WN) recorded at LA - 116th St School.

The importance of higher modes can be observed by evaluating the behavior of the 6-story frame (Figure 5.2b). In this case, the structure is tuned to a fundamental period in the vertical direction equal to $T_{1v} = 0.15\,\mathrm{s} = {}^{20}/_{3}\,\mathrm{Hz}$ (see Table 4.3. This period lies exactly on the lower corner frequency of the NEHRP-spectrum in Figure 2.1. Thus, the first few higher modes of the 6-story structure experience relatively high modal spectral acceleration demands, which cause an increase in accelerations with respect to the 3-story structure. This behavior is also observed for the 12- and 20-story generic stick models.

These results show that, in general, PFA_v tend to vary linearly over the structure's height. The taller the structure, the more S-shaped the PFA_v profiles are. This behavior is also reported in a study of Chaudhuri and Hutchinson [35] on the evaluation of PFA_h demands. While regression equations are proposed for the S-shaped PFA_h demand in [35], a very simple linear fitting equation could lead to a useful approximation of the PFA_v demands over the height of the structure.

Using the NEHRP-spectrum compatible record leads to an adequate approximation of the median profile for the 3- and 6-story structure (see Figures 5.2a and 5.2b). However, the median

PFA_v demand of the 12-story structure is slightly overestimated and the profile of the 24-story frame is underestimated at most levels along the height of the structure. This phenomenon could be explained by evaluating the objective function in Equation (2.2) in the frequency range between $^{10}/_{3}\,\text{Hz} \leq f_v \leq 40\,\text{Hz}$, as discussed in Section 2.2 and shown in Figure 2.2. The higher modes of the 12- and 24-story structure exceed the upper limit of $f_{v,up} = 40\,\text{Hz}$, in particular, the 7th frequency of the 12 story frame equals $f_{v7}^{(12story)} = 44.54\,\text{Hz}$. However, a further study is required to show precisely the contribution of high frequent modes to the PFA_v response and their affect on the evaluation of the objective function in Equation (2.2).

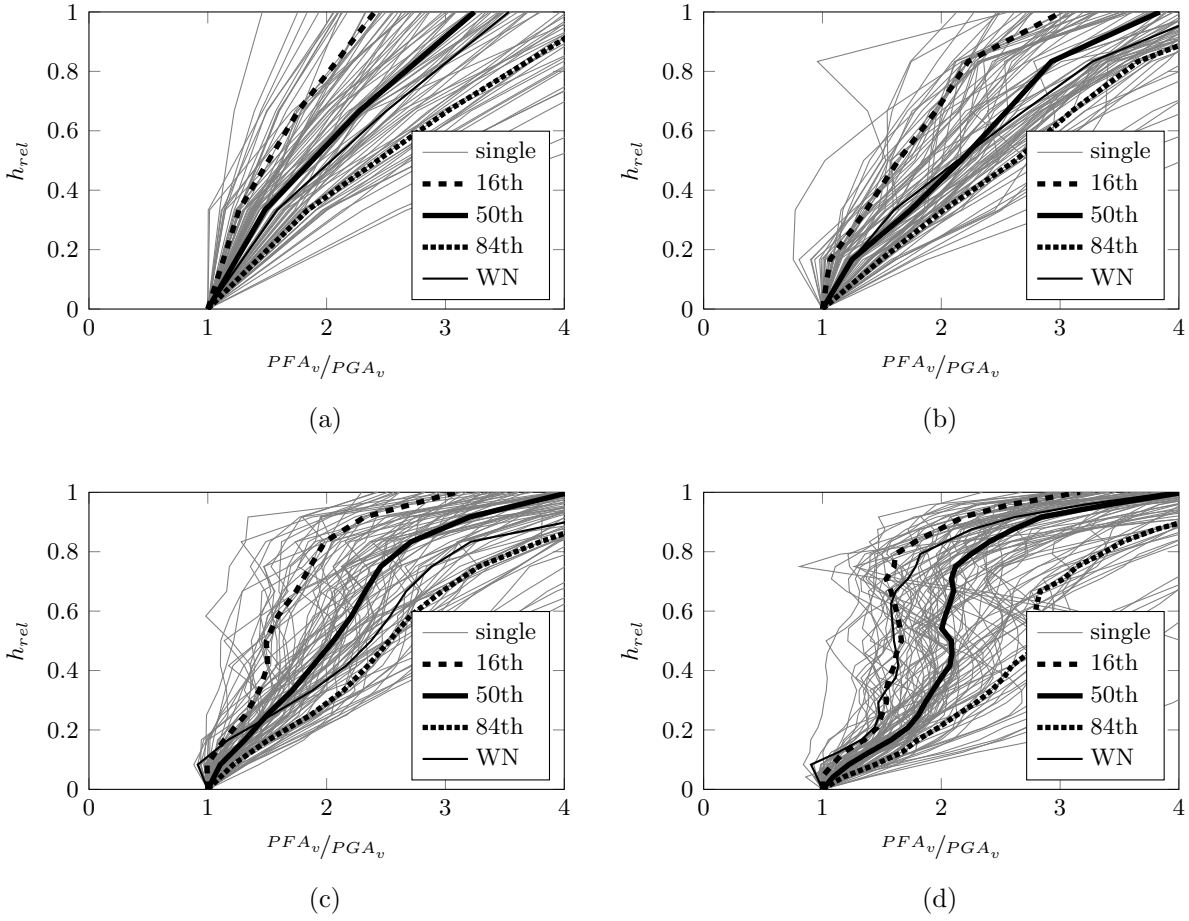

Figure 5.2: Profiles of the vertical peak floor acceleration demand normalized to the vertical peak ground acceleration for the (a) 3-story, (b) 6-story, (c) 12-story, and (d) 24-story generic stick models exposed to records from the VGM record set and the single record from the Whittier Narrows earthquake (WN) recorded at LA - 116th St School.

In order to evaluate the adequacy of Equation (1.1), which was developed for NSCs [1], Figure 5.3 shows the ratio of PFA_v to PGA_h. The vertical dash-dotted line at $^{PGA_v}/_{PGA_h} = {}^{1}/_{2}$ represents Equation (1.1) in terms of the vertical acceleration demand of a nonstructural component based on seismic design provision in the United States. It is evident from Figure 5.3 that the codified procedure leads to an underestimation of the PFA_v demand in contrast to the median profiles. As already mentioned, a linear variation of PFA_v over the height is a more accurate estimation. A reasonable distribution analogue to the PFA_h (i.e. height factor)

demand determined from the seismic equivalent lateral forces acting on NSCs defined in [1] would probably lead to a better approximation based on the results from this study.

At the base of the structures, the resulting PFA_v to PGA_h ratios are consistent with the V/H ratios discussed in the study of Bozorgnia and Campbell [7] regarding the V/H ratio. Traditionally, the $^{PGA_v}/_{PGA_h}$ ratio is assumed to be $^2/_3$, which is adequate for a median ratio. However, the 84th percentile value is larger than unity and the peak value is larger than two. Therefore, if the objective is to propose a codified procedure to estimate V/H ratios, a value greater than $^2/_3$ may be warranted.

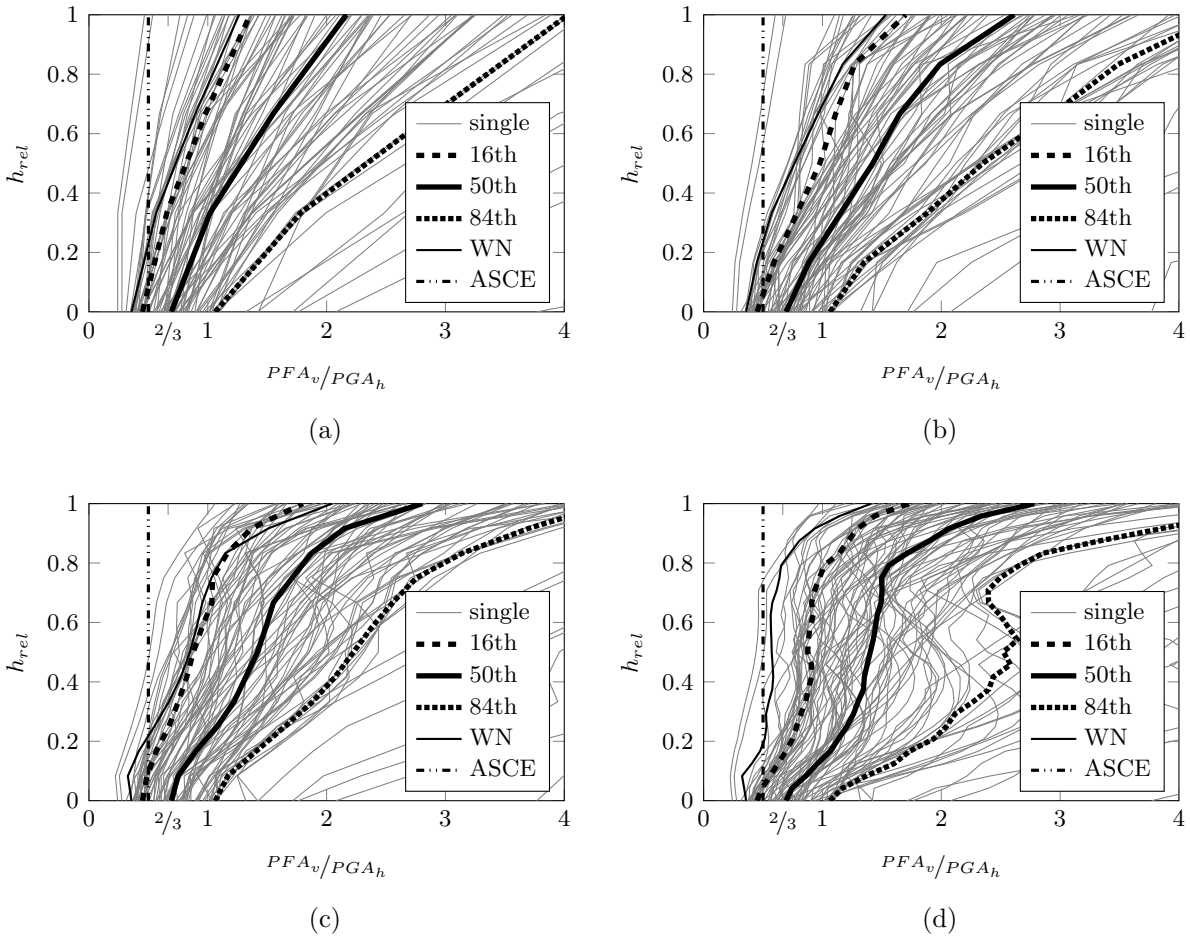

Figure 5.3: Profiles of the vertical peak floor acceleration demand normalized to the horizontal peak ground acceleration for the (a) 3-story, (b) 6-story, (c) 12-story and (d) 24-story generic stick models exposed to records from the VGM record set and the single record from the Whittier Narrows earthquake (WN) recorded at LA - 116th St School.

The NEHRP-spectrum compatible single record leads to an inaccurate estimate of the $^{PGA_v}/_{PGA_h}$ ratio (thin black line). This ratio was not accounted for in the objective function in Equation (2.2), which was used to obtain the spectrum-compatible single record. In Figure 5.3 it can be seen if the profiles obtained from the single record are translated to match $^{PGA_v}/_{PGA_h} \approx {}^2/_3$ the fit with the median profile of the VGM record set is greatly improved. This shift can be interpreted as a *missing* objective function or as a *missing constraint* in the existing objective function.

6 Summary and Conclusion

The focus of this report is on the evaluation of vertical peak floor acceleration demands in regular perimeter frames of steel structures designed according to older [20] and more modern generations of U.S. design codes [22]. A design engineer relies upon available seismic standards [1, 3] to estimate different response quantities, e.g. displacement-, drift- and horizontal acceleration demands for floor diaphragms and nonstructural components (NSCs). However, rigorous treatment of the vertical peak floor acceleration (PFA_v)demand on NSCs is neglected in the aforementioned codes since typical civil engineering structures are assumed to behave rigid in vertical direction.

This study highlights in the introduction critical research needs as well as the importance of studying PFA_v demands for NSCs. The most salient observation from the results of this study is that neglecting the vertical component of the base acceleration may lead to a drastic underestimation of the design forces for NSCs. Since repair costs associated with seismic damages to NSCs could be as high as 92 % of the total repair costs (e.g. for a hospital) [36], understanding and quantifying component vertical acceleration demands becomes a relevant issue.

Therefore, in the second chapter, a record set compatible to the recommended vertical design response spectrum in the United States [8] (in this report referred as NEHRP-spectrum) is created. Additionally, a single record matching the NEHRP spectrum is also obtained to evaluate median demands with relative ease.

The third chapter deals with the design of perimeter frames of real steel-frame structures in order to evaluate modal properties, in particular relations between the fundamental period in horizontal T_{1h} and vertical T_{1v} direction and the number of stories N, as well as the statistical evaluation of the spatial variation of their corresponding mode shapes.

In chapter four a generic stick model is presented based on the observations of the real frame structures to perform parametric studies. These generic structures were used to evaluate PFA_v demands close to the locations of columns in the structure.

Finally, the fifth section combines the information of the generic models and the vertical ground motions. Therefore, the generic stick models with 3-, 6-, 12- and 24-stories are generated and excited at their base separately by the vertical and horizontal ground motion records of the NEHRP-spectrum compatible record set and the NEHRP-spectrum compatible single record. The results show that the vertical floor acceleration demands are in general much greater (up to a factor of three in the median) than the peak vertical ground acceleration. In addition, peak vertical floor accelerations tend to increase with height. These two observations are not explicitly accounted for in current design provisions in the United States, which may lead in many cases to the underestimation of vertical component design forces. However, these conclusions are based on assumptions made on numerical models and ground motion properties consistent with the ones used in this study. In addition, only record-to-record variability was accounted for.

Future studies should account for the following issues in order to provide sufficient data to be able to make more general conclusions:

- Simplified modeling of vertical peak floor acceleration demands for components located close to columns of the gravity system.
- Quantification of the dynamic characteristics of girders/slabs on vertical peak floor acceleration demand at open-bays ($PFA_v^{(bay)}$).
- Determination of the floor response spectra close to columns and at open-bays.
- Generation of simplified equations to estimate $PFA_v^{(col)}$ and $PFA_v^{(bay)}$ demands as well as the estimation of floor response spectra in those regions.

7 Bibliography

[1] ASCE. *Minimum Design Loads for Buildings and Other Structures*. [Reston and Va.], 2010.

[2] International Code Council. *International Building Code*. 2012.

[3] Österreichisches Normungsinstitut. *ÖNORM EN 1998-1: EUROCODE 8: Teil 1: Grundlagen, Erdbebeneinwirkungen und Regeln für Hochbauten*. 2013-06-15.

[4] Wieser, J. D., Pekcan, G., Zaghi, A. E., Itani, A. M. and Maragakis, E. "Assessment of Floor Accelerations in Yielding Buildings". In: *MCEER reports*. Ed. by University at Buffalo, State University of New York. Vol. Technical Report MCEER-12-0008. MCEER Report.

[5] ICC-ES. *Acceptance Criteria for Seismic Qualification by Shake-Table Testing of Nonstructural Components and Systems*. 2007-06-01.

[6] Campbell, K. W. and Bozorgnia, Y. (2003). Updated Near-Source Ground-Motion (Attenuation) Relations for the Horizontal and Vertical Components of Peak Ground Acceleration and Acceleration Response Spectra. *Bulletin of the Seismological Society of America* **93**: 314–331.

[7] Bozorgnia, Y. and Campbell, K. W. (2004). The Vertical-to-Horizontal Response Spectral Ratio and Tentative Procedures for Developing Simplified V/H and Vertical Design Spectra. *Journal of Earthquake Engineering* **8**: 175–207.

[8] Applied Technology Council. *NEHRP Recommended Seismic Provisions for New Buildings and Other Structures*. 2009.

[9] USGS. *Geologic Hazards Science Center: U.S. Seismic Design Maps*.

[10] Campbell, K. W. and Bozorgnia, Y. (2008). NGA Ground Motion Model for the Geometric Mean Horizontal Component of PGA, PGV, PGD and 5% Damped Linear Elastic Response Spectra for Periods Ranging from 0.01 to 10 s. *Earthquake Spectra* **24**: 139–171.

[11] Seifried, A. E. "Response Spectrum Compatibilization and its Impact on Structural Reponse Assessment". PhD thesis. Stanford CA: Stanford University, 2013.

[12] Pacific Earthquake Engineering Research Center. *PEER Ground Motion Database*. 2010.

[13] Joyner, W. B. and Boore, D. M. (1981). Peak Horizontal Acceleration and Velocity from Strong-Motion Records Including Records From the 1979 Imperial Valley, California, Earthquake. *Bulletin of the Seismological Society of America* **71**: 2011–2038.

[14] Campbell, K. W. and Bozorgnia, Y. "Engineering Characterization of Ground Motion". In: *Earthquake Engineering*. Ed. by Bozorgnia, Y. and Bertero, V. V. CRC Press, 2004.

[15] The MathWorks Inc. *MATLAB*. 2013.

[16] Heo, Y., Kunnath, S. K. and Abrahamson, N. (2011). Amplitude-Scaled versus Spectrum-Matched Ground Motions for Seismic Performance Assessment. *Journal of Structural Engineering* **137**: 278–288.

[17] Shome, N. "Probabilistic Seismic Demand Analysis of Nonlinear Structures". PhD thesis. Stanford CA: Stanford University, 1999.

[18] NIST National Institute of Standards and Technology. *Selecting and Scaling Earthquake Ground Motions for Performing Response-History Analysis*. Gaithersburg and MD, 2011.

[19] Abraham, A., Jain, L. C. and Goldberg, R. *Evolutionary Multiobjective Optimization: Theoretical Advances and Applications*. New York: Springer, 2005.

[20] International Conference of Building Officials. *Uniform Building Code Vol. 2 – Structural Engineering Design Provisions*. 1994.

[21] Gupta, A. "Seismic Demands for Performance Evaluation of Steel Moment Resisting Frame Structures". PhD thesis. Stanford CA: Stanford University, 1999.

[22] International Code Council. *International Building Code*. 2009.

[23] Applied Technology Council. *Evaluation of the FEMA P-695 Methodology for Quantification of Building Seismic Performance Factors*. 2010.

[24] CSI. *SAP2000*. Walnut Creek CA.

[25] Applied Technology Council. *Quantification of Building Seismic Performance Factors*. 2009.

[26] ASCE. *Minimum Design Loads for Buildings and Other Structures*. [Reston and Va.], 2005.

[27] American Institute for Steel Construction. *Seismic Provisions for Structural Steel Buildings*. 2005.

[28] American Institute for Steel Construction. *Prequalified Connections for Special and Intermediate Steel Moment Frames for Seismic Applications*. 2005.

[29] Medina, R. A. "Seismic Demands for Nondeteriorating Frame Structures and Their Dependence on Ground Motions". PhD thesis. Stanford CA: Stanford University, 2003.

[30] Sankaranarayanan, R. "Seismic Response of Acceleration-Sensitive Nonstructural Components Mounted on Moment-Resisting Frame Structures". PhD thesis. College Park Maryland: University of Maryland, 2007.

[31] Clayton, J. S. "Probabilistic Seismic Hazard Analysis for Acceleration-Sensitive Nonstructural Components Attached to Shear Wall Structures". MA thesis. Durham: University of New Hampshire, 2010.

[32] Medina, R. A., Sankaranarayanan, R. and Kingston, K. M. (2006). Floor Response Spectra for Light Components Mounted on Regular Moment-Resisting Frame Structures. *Engineering Structures* **28**: 1927–1940.

[33] Miranda, E. and Taghavi, S. (December 9-11, 2009). A Comprehensive Study of Floor Acceleration Demands in Multi-Story Buildings. In: *ATC and SEI Conference on Improving the Seismic Performance of Existing Buildings and Other Structures*; 616–626 pp.

[34] Lòpez-García, D., Price, P., Torrejón, E., Vial, F. and Wichmann, P. (2008). Peak Floor Accelerations in Multistory Buildings Subjected To Earthquakes. In: *Proceedings of the 14th World Conference on Earthquake Engineering*; pp.

[35] Chaudhuri, R. S. and Hutchinson, T. C. (2004). Distribution of Peak Horizontal Floor Acceleration for Estimating Nonstructural Element Vulnerability. In: *Proceedings of the 13th World Conference on Earthquake Engineering*; pp.

[36] Taghavi, S. "Response Assessment of Nonstructural Building Elements". PhD thesis. Stanford CA, 2003.